TTC003 – Final Year Project Report

Autonomous Electric Bicycle

Vincent J. Renders[1]
Department of Aeronautical and Automotive Engineering,
Loughborough University, Loughborough, Leicestershire LE11 3TU, UK

Bicycles are an extremely efficient form of transportation due to their low energy costs and small system profiles. A fleet of autonomous, electric or fuel cell powered two-wheeled vehicles, transporting people or goods, could form one part of an elegant solution to solve congestion problems in cramped urban spaces, ultimately helping to create a safer, cleaner and heathier living environment for its inhabitants. This is the context of the project and the requirements for such a transport method are threefold; the vehicle must be self-balancing in steady motion, self-balancing during manoeuvres and able to follow a pre-programmed or controlled path. A solution to the first two of these is being attempted in this assignment.

Bicycles balance by steering into the direction of undesired lean therefore an autonomous bicycle, or two-wheeled vehicle, must operate using the same principle. At a given speed, the vehicle should be capable of applying a torque, that is related to the vehicle's attitude, to the steering axis by some means of actuation. In this project, actuation of the steering is provided by a DC motor, the torque output of which is controlled by a PID control system as a function of the motor supply voltage. The attitude estimation is provided by a set of calculations and algorithms that filter readings from an inertial measurement unit to compute a reliable approximation for the roll angle of the vehicle.

The outcome of this work includes the production of a prototype instrumentation device with the accompanying calculations that provide the roll angle estimation required for control of the vehicle. In addition, inroads into the control system of an autonomous, two-wheeled vehicle are made, combining a computational model of a motorcycle and one of a DC motor, simulating the application of steering torque and its capabilities as a means of steering actuation.

---

[1]Aeronautical Engineering BEng; B627526; Project supervisor: Dr Georgios Mavros MSc., PhD

Table of Contents

Nomenclature

Symbols & Notation

x – horizontal axis in direction of motion

y – horizontal axis perpendicular to motion

V – velocity

z – vertical axis perpendicular to motion

a – acceleration

g – surface acceleration due to gravity

R – radius

ε – caster angle

m – mass

a – trail

p – wheelbase

d – fork offset

β – seat post angle

δ – steering angle

ψ – yaw/turning angle (rotation about z)

φ – roll angle (roll about x)

θ – pitch angle (pitch about y)

ω – angular velocity

Abbreviations, Prefixes & Colloquialisms

i-Bike – *instrumented* bicycle

e-Bike – *electric* bicycle

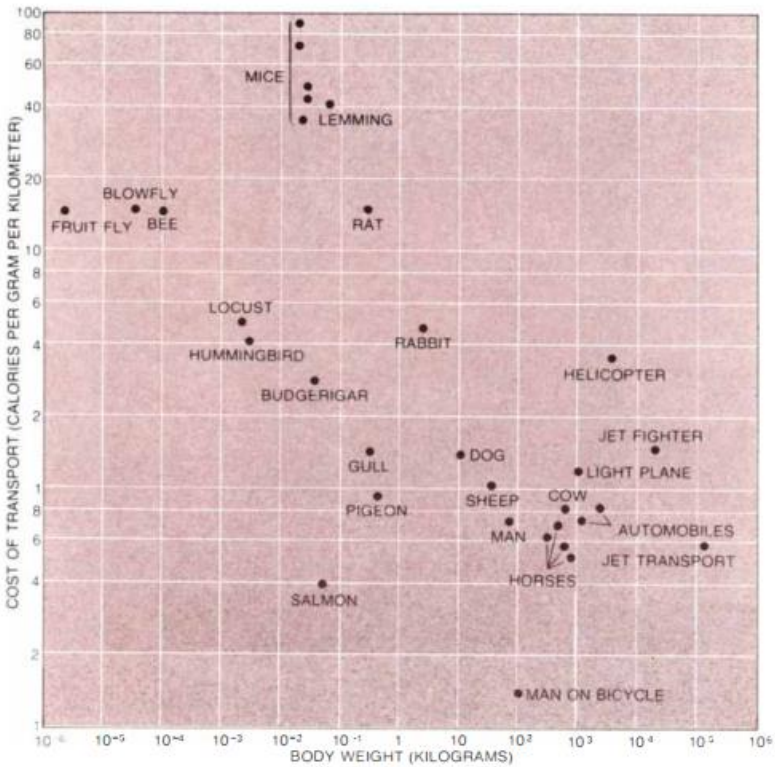

MAN ON A BICYCLE ranks first in efficiency among traveling animals and machines in terms of energy consumed in moving a certain distance as a function of body weight. The rate of energy consumption for a bicyclist (about .15 calorie per gram per kilometer) is approximately a fifth of that for an unaided walking man (about .75 calorie per gram per kilometer). With the exception of the black point representing the bicyclist (*lower right*), this graph is based on data originally compiled by Vance A. Tucker of Duke University.

Figure 1 - Chart presented by S.S. Wilson in the March 1973 issue of *Scientific American*.[1]

1 Introduction to the Autonomous Electric Bicycle

The modern bicycle is the most efficient method of transport in terms of energy cost, as a function of system mass, in history. This fact was shown by S.S. Wilson in the March 1973 issue of *Scientific American* when he had the insight to test the efficiency of such a machine with a human rider and add this single point, labelled "Man on Bicycle", to a chart created by researchers studying the locomotion efficiencies of animals and machines. This efficiency is due to the human ability to generate power by converting sustainable fuel sources into mechanical work in the muscles, and the low resistances of travel combined with the extremely high efficiency of the power transmission mechanisms of the bicycle, in the region of 80-98%.[2]

As well as being among the most efficient means of transport ever in terms of energy cost per kilogram of system mass, two-wheeled vehicles, and human propelled bicycles especially, are efficient in other ways. Their small physical profiles give them advantages such as low drag penalties, greater manoeuvrability, road access and power to weight all at a reduced cost. In other words, they come into their own over relatively short ranges and in urban settings.

Most towns and cities suffer from severe congestion due to a combination of human behaviours and inflexible environments, particularly in old, historic cities. Use of fossil fuels as an energy source and the supposed convenience they offer, and the transport modes they power, come at the cost of the health and quality of life of the inhabitants as a result of subsequent air and noise pollution. An autonomous, sustainably powered, two-wheeled vehicle could present a solution to this problem if fleets of them became a mainstream method of delivering people or goods in urban areas.

Subsequently, this is where this project finds its context. Its early objectives, as requirements for such a transport medium are threefold; self-balancing in steady motion, self-balancing during manoeuvres and able to follow a pre-programmed or controlled path, the first two of these challenges are being undertaken in this assignment. As such, this project has two aims:

1. Explore the use of a simple PID controller to give a bicycle balance stability and steady state turning capabilities analytically, using theoretical and computational methods.
2. Consider ways to practically implement a controller, as described above, to balance a conventional bicycle and function as a proof of concept to the solution described above.

These aims have been divided further into quantifiable objectives, the completion of which would lead to the concept's development and are as follows:

- Model a DC motor that produces torque as a function of voltage supplied.
- Integrate the model above into the motorcycle model as the steering actuator.
- Adapt a pre-existing vehicle model to replicate true properties of the test bicycle
- Complete tuning of PID gains, simulating the above model, for optimum performance
- Design & test the roll angle and velocity sensor module as well as the steering actuation
- Install the control system components on board the test vehicle.

External circumstances have forced the original quantifiable objectives to be reassessed and the corresponding tasks and plan of works to be adapted accordingly. Information and the context of such changes are documented in detail at the beginning of the appendix.

The first section that follows this introduction outlines the academic background of the subject, providing context for the work being undertaken and insight into the relevant technical topics that are involved in doing so. The three sections after that present the technical progress made towards the completion of a working prototype of the concept above, specifically in areas such as computational modelling, installation of necessary hardware for roll angle estimation, as well as the accompanying computational algorithms required to compute this estimation.

2 Dynamics & Control of a Bicycle

2.1 Bicycle Geometry & Modelling

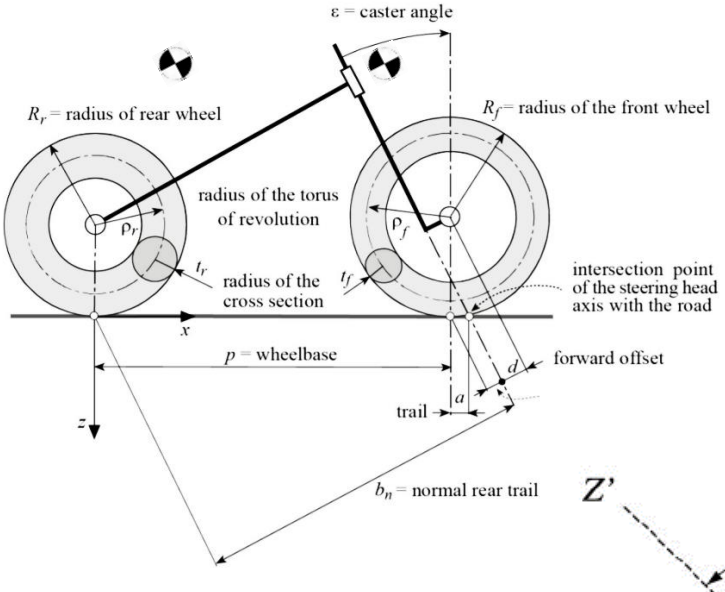

Figure 2 – Left: Figure adapted from *Cossalter et al.*[6] depicting the simplified bicycle models, its geometry properties and the centres of mass & inertia axes of the front and rear assemblies. Both wheels each have a spin moment of inertia that exhibit gyroscopic behaviours.

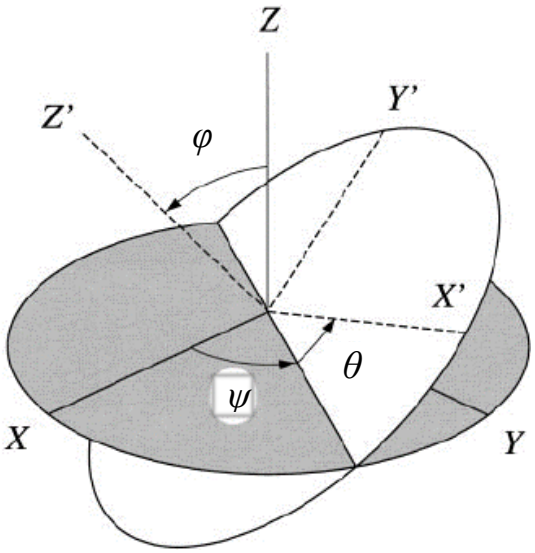

Figure 3 – Right: Euler angle notation employed for modelling of this project. Adapted from *Zhang & Sejnowski, 1999*.[7]

In the interests of clarity, notation of the bicycle's co-ordinate systems, body frames of reference and notable features of its geometry are defined here, in writing, in the figures above and in the Nomenclature. The definitions here apply to the content in all sections that follow, and the author recommends that readers refer to them when necessary.

When describing the motion of a vehicle, two frames of reference are used: the global reference (the grey plane in figure 3) and the body reference (the white plane in figure 3). The attitude of a body (the bicycle) with respect to the global reference frame can be expressed using the aircraft Euler angles; roll (φ), pitch (θ) and yaw (ψ). In the body reference frame, the X axis is the direction of travel where forward is positive, Y is the lateral axis that is positive to the left, and Z is the vertical axis where downwards is the positive direction. A vector in the body reference system, $\overline{\boldsymbol{u}}_B$, can be converted into its equivalent in the global reference system, $\overline{\boldsymbol{u}}_G$, using a rotation matrix as follows:

$$\overline{\boldsymbol{u}}_B = R_\psi R_\theta R_\varphi \overline{\boldsymbol{u}}_G \qquad (1)$$

where,

$$R_\psi = \begin{bmatrix} \cos\psi & -\sin\psi & 0 \\ \sin\psi & \cos\psi & 0 \\ 0 & 0 & 1 \end{bmatrix}, \quad R_\theta = \begin{bmatrix} \cos\theta & 0 & \sin\theta \\ 0 & 1 & 0 \\ -\sin\theta & 0 & \cos\theta \end{bmatrix}, \quad R_\varphi = \begin{bmatrix} 1 & 0 & 0 \\ 0 & \cos\varphi & -\sin\varphi \\ 0 & \sin\varphi & \cos\varphi \end{bmatrix}$$

A property of bicycle geometry that is worth noting due to its relevance to this work is the *trail*, *a*, which can be seen in Figure 2. The trail of a bicycle is defined as the perpendicular distance from the contact point made by the front wheel to the point at which the steering axis intersects the ground.[2] Trail is defined as positive if the steering axis-ground intersection is in front of the contact point made by the front wheel. Generally, the more positive the trail of a bicycle, the more stable it is when ridden and vice versa. This is merely an early introduction to this particular characteristic; its significance is covered in greater detail in the next section.

The mass of the rider is by far the most important component of the total system mass of a bicycle. Since modelling completed in this work considers a conventional, rider-less bicycle, the rider mass is neglected, which allows some simplifications to be made. Without the rider, and hence without the most important influences on aerodynamic drag and rolling resistance, both components will be smaller. Aerodynamic losses are proportional to the frontal area, which is drastically reduced once the rider is removed, and the square of the forward velocity, which is also smaller at low forward velocities. As this model will be tested at low speed ($<<10$ m s^{-1}) and the remaining frontal area of the bicycle is relatively small, aerodynamic losses can be neglected.

Rolling resistance encompasses tyre resistance and ground resistance,[2] both of which increase with vehicle mass and are assumed to be small after removing the rider. Any further resistance components from slopes and deformation of the surface are eliminated by assuming a smooth and level road surface. Furthermore, tyres are modelled as thin disks with negligible gyroscopic effects. The conscious and subconscious biomechanical control inputs made by a rider, such as body lean and pedalling that affect the centre of mass position, and subsequently the motion and handling characteristics of the bicycle, are also omitted following the removal of the rider. During manoeuvres, such as the steady turn, the steering angle, δ, of the front wheel is small.

Generally, models of motorcycle dynamics are also applicable to bicycles, the only differences being some parameters such as system mass, centre of mass location, moments of inertia, typical speed of travel, swingarm & suspension dynamics and vehicle geometries, all of which can be compensated for, following extensive reparameterisation. All assumptions made for modelling purposes, and described here, have been validated experimentally[13] and shown in literature to be admissible for a rider-less bicycle travelling with a forward velocity of up to 6 m s^{-1},[14] as is, or will be, the case in this work.

2.2 Bicycle Dynamics – or How to Balance a Bicycle

The dynamics of a bicycle form the foundation this project and an appropriate understanding of them underpins all subsequent work. Due to the complex mathematics and the number of subtle concepts involved, bicycle dynamics have not been thoroughly researched until relatively recently, yet they still remain a minefield of ambiguity and popular misconception outside the relevant academic circles.

One of the earliest and most famous works on the subject is the '*Whipple bicycle*' model, first presented by Francis Whipple in 1899,[8] in which he uses a simplified model of a bicycle and rigid body dynamics to establish two general, fundamental concepts that are still accepted today:

1. A rider balances a forward travelling, conventional bicycle by steering into the direction of undesired lean, thus, laterally accelerating the support points in contact with the ground beneath the centre of mass of the rider/bicycle system.
2. An uncontrolled, conventional bicycle travelling at a speed of approximately 6 m s^{-1} (21.6 km h^{-1}) can balance itself until its velocity decays below a certain level.

These principles are basic starting points but the more recent works of *Jones 1970*[11] and *Papadopoulos et al.* 2007[14] expand on this and contain the most valuable lessons for obtaining the required understanding specific to the subject being undertaken. From extensive experimentation, Jones observes that a conventional bicycle, with positive trail geometry and travelling with sufficient velocity, will balance itself due to the self-correcting steering torques that are generated by the caster effect of the bicycle's front assembly, which is itself a result of the positive trail. It is the caster effect of a conventional bicycle's frontal assembly that tends to keep the heading of the wheel in the direction of travel of the system, preventing the tracks of the wheels from diverging and thus allowing the bicycle to be stable and self-balancing.

Jones also observes that the contributions of the gyroscopic effects of the wheels, to the stability of a bicycle, are small which is supported by *Papadopoulos et al.* 2007 who suggest that, in addition to any gyroscopic and caster effects, it is myriad factors that contribute to stability. According to them, the other contributions include the centre of mass locations of the front and rear frames, their corresponding moments of inertia and the head angle, a geometric property of the bicycle. The value of Jones' work to this project is attributed to the use of a conventional bicycle in the experiments that inform his conclusions. As a conventional bicycle is also being used here, his conclusions are highly relevant to the modelling and parameterising of the bicycle at a general level. The works of *Papadopoulos et al.* affirm the assumptions made when modelling the bicycle and their linearised dynamic equations can be employed for the benchmarking of a control system.

2.3 Steering Torque – or How to Steer a Bicycle

Civil engineer W.J.M. Rankine was the first observe the application of a steering torque,[15] in the context of counter steer, to initiate the lean involved in the turning manoeuvre of a bicycle. When executing a left turn, the rider of a bicycle will first torque the handlebars fractionally to the right, often without realising, causing the bicycle to start to lean to the left. Soon after, they then torque handlebars back to the left in the direction they want to turn, stabilising the motion by accelerating the contacts of the wheels toward the point below the centre of mass, but not so much that the lean is eliminated. The centrifugal, gravitational and contact forces all become balanced and the bicycle turns (see section 2.4 for further detail on dynamics of the steady turn).

As covered in the previous section, the front wheel of the bicycle tends to reorient in the direction of motion due to the caster and gyroscopic effects of the front wheel. Therefore, to complete a turning manoeuvre, a torque that opposes these effects, plus those from the ground due to the friction of the tyre, must be applied to the steerer and maintained. For a rider-less, two-wheeled vehicle, the only available control input of the vehicle is the steering torque, which is calculated using the roll angle estimation and PID control and delivered by the DC motor(s) as the final output of the control system. Reassuringly, *Schwab et al.*[19] confirm analytically that a bicycle can be fully controlled by steering torque exclusively.

2.4 The Steady Turn Case

The steady turn is a special case in bicycle dynamics where the out-of-plane dynamics are in a state of roll equilibrium;[21] the bicycle system is travelling at speed, V_x, leaning with a roll angle, φ, following a circular path with radius, R_c, such that the moments, centrifugal, gravitational and wheel contact forces are all balanced, as shown in Figure 4. The roll angle, φ, required for a bicycle to complete a steady turn of radius, R_c, for a given forward velocity, V_x, can be derived (refer to Appendix 1 for the complete derivation) and given generally by equation 2, in terms of forward velocity & yaw/turn rate by equation 3 and, finally, in terms of forward velocity and turn radius by equation 4.

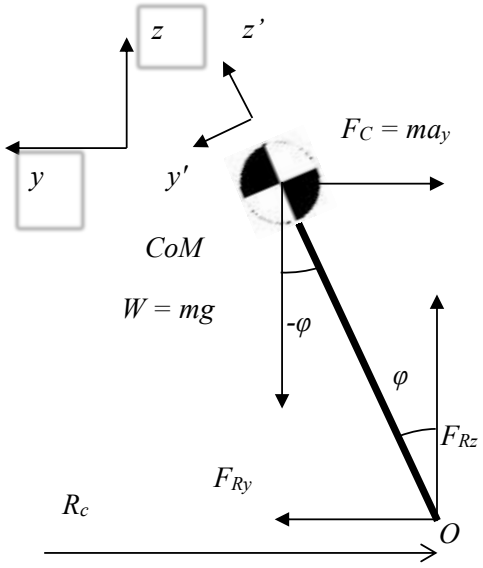

Figure 4 – Free body diagram of the steady turn case. The forces at work in this system are the centrifugal forces, F_C, from the lateral acceleration of the turn, the weight acting through the CoM, W, and the reaction & frictional forces from the tyre contacts, F_{Ry} and F_{Rz}. Roll angle, φ, is the angle made about the x-axis by the plane of the bicycle frame from the horizontal. For further notes, refer to Appendix 1.

$$\varphi = \tan^{-1}\left(\frac{a_y}{g}\right) \qquad (2)$$

$$\varphi = \tan^{-1}\left(\frac{V\dot{\psi}}{g}\right) \qquad (3)$$

$$\varphi = \tan^{-1}\left(\frac{V^2}{R_c g}\right) \qquad (4)$$

For practical purposes, equations 3 & 4 are the most useful for this application, since the variables of equation 3, forward velocity, V, and yaw rate, $\dot{\psi}$, are easily measurable. The turn radius, R_C, which features in equation 4 is less evident in practice, however, if the path of an autonomous bicycle could be generalised as a number of a steady turns, n, of a specified radius R_{Cn},[18] the roll angle, φ, required for these turns can be calculated. From this, the turns could be executed by the controller, delivering the necessary steering torque and, hence, following the path that has been programmed.

Furthermore, this exercise allows one to consider the system as a closed, feedback loop, where the pilot or controller of a bicycle executing a steady turn is, at any given time, applying a torque to correct the error between the required roll angle and the actual roll angle, as perceived or measured by the pilot or controller respectively.[17] One can extend this exercise to the steady forward motion case, as well as the steady turn, where the required roll angle is equal to zero and must be kept constant.

2.5 Roll Angle Estimation & Instrumented Bicycles

Roll angle is the vital state input for the control system. More specifically, it is the error between the required roll angle and the actual roll angle that informs the required steering torque required for a given manoeuvre. As such, a reliable estimation for this variable is mandatory. When it comes to instrumenting bicycles, affectionately dubbed 'iBikes,'[19] the literature is thorough, and the most common approach is to use micro-electromechanical systems (MEMS) to take measurements directly. Using sensors, specifically accelerometers and gyroscopes, and a series of calculations using the measurements taken, an estimation of the roll angle can be obtained. This technical approach is covered in depth in section 5 of this document.

Another important variable for the of roll angle estimation and general control of the vehicle is the forward velocity, given by equation 5, calculated using the radius, R_{wr}, and angular rate ω_{wr}, of the rear wheel. The angular velocity is obtained using a small magnet attached to the spokes of the rear wheel and a Hall Effect sensor attached to the bicycle frame, a method not renowned for accuracy but deemed as more than adequate for a bicycle application.[20]

$$V = -\omega_{wr} R_{wr} \qquad (5)$$

2.6 PID Control & DC Motors for Steering Actuation

As previously stated, steering torque is the only way of controlling a rider-less bicycle. DC motors are a desirable actuator for this application as the shaft torque is the output that must be controlled, whereas a servo or stepper motor can only control shaft position. Steering a bicycle involves torqueing the handlebars to the left and to the right, and this is no different for an electronic controller.

The motor delivering the torque should therefore be controllable bidirectionally and it is possible to achieve this using DC motors and a device known as an H-bridge to reverse the polarity of the voltage across the motor on command and, hence, change the shaft's direction of rotation. For the torque to be delivered across two parallel shafts, the motor shaft and the steerer tube of the bicycle, a gear or belt drive mechanism will be required and may have a ratio to amplify or reduce the torque being delivered.

PID control accurately reflects the ability of a human rider,[17] whose reflex & skill delivers the accuracy and responsiveness of stabilising a bicycle in motion and in the presence of external disturbances. PID control is a three-term controller that stands for proportional (P) plus integral (I) plus derivative (D) control. Proportional feedback is when the feedback control signal is directly proportional to the error, using a linear constant k_P for the gain. The resulting system is highly responsive but is more likely to become unstable if the proportional gain is too high. Addition of an integral term insulates the system, allowing it to maintain a steady state error of zero even in the presence of external disturbances but can lead to a greater overshoot and a dynamic response of the system. The integral term is represented by $k_I s^{-1}$. Finally, the inclusion of a derivative term, k_D, stabilises the system, but reduces its responsiveness.[24]

With velocity and roll angle estimations available, the desired steering torque can be computed using a PID control system onboard a microcontroller and applied using the DC motor as mentioned previously. The controlling signal can be transmitted as a pulse width modulated output from the microcontroller unit, moderating the voltage supplied to the motor and, thus, regulating its output torque & direction of rotation.[25]

3 Computational Modelling of a Motorcycle with Actuated Steering

The modelling, tuning and reparametrising of a motorcycle that uses a DC motor for steering actuation, as the sole control input to the vehicle, forms a significant portion of this work and is the subject of this section. The control system is the heart of any autonomy-enabled vehicle. Computational tools, like *Simulink*, are hugely advantageous for building such control models and offer the ability to tune the gains of the model to obtain the optimal, desired characteristics for the behaviour of its output. These characteristics include, but are not limited to, the following: rise time, settling time, overshoot, peak time, stability, dynamic response and any error in the signal.

3.1 DC Motor Dynamics

In the previous sections, steering torque was discussed as the method for controlling the steering of a bicycle, with DC motors and their governable torque output, as the appropriate actuator for such a task. Torque output, as a function of the voltage supplied, is practical for this application since the voltage supply can be managed by the control system and modulated by a microcontroller. Obtaining such a function requires some manipulation of the governing equations of DC motors; differential equations 11 & 12 describe their electrical and mechanical behaviour in terms of both the circuit and the motor properties.[23]

Equation 6 is derived from application of Kirchhoff's Voltage Law of the DC motor equivalent circuit model and relates the input voltage supply to the rotational speed, ω, output by the motor in terms of the current, i, resistance, R, the inductance of the coils, L, and the back EMF which is proportional to the rotational speed output.

Equation 7 is derived using Newton's Law applied to one dimensional rotation and relates the torque output, proportional to the current, to the moment of inertia of the load on the shaft and to the change of rotational speed with time. These can be manipulated and used as state space model equations to model a motor, using its known properties, in *Simulink* to predict its outputs. From these, a transfer function of the DC motor dynamic model can be obtained.

$$v_0(t) = i(t)R + L\frac{di(t)}{dt} + k_B\omega(t) \quad (6)$$

$$I_L\frac{d\omega(t)}{dt} = k_T i(t) \quad (7)$$

The manipulation of equations 6 & 7 and the resulting *Simulink* motor model follows below. Rearranging both of the above to get the derivative terms on one side gives:

$$\frac{di(t)}{dt} = \frac{1}{L}(v_0(t) - i(t)R - k_B\omega(t)) \quad (6a)$$

$$\frac{d\omega(t)}{dt} = \frac{k_T}{I_L}i(t) \quad (7a)$$

Integrating the above with respect to time, t, gives:

$$\int_0^t \frac{di(t)}{dt}dt = \frac{1}{L}\int_0^t (v_0(t) - i(t)R - k_B\omega(t))\,dt \quad (6b)$$

$$\int_0^t \frac{d\omega(t)}{dt}dt = \int_0^t \frac{k_T}{I_L}i(t)\,dt \quad (7b)$$

Assuming initial conditions are equal to zero when $t = 0$, leaves the integral functions below:

$$i(t) = \int \frac{1}{L}(v_0(t) - i(t)R - k_B\omega(t)) \quad (8)$$

$$\omega(t) = \int \frac{k_T}{I_L}i(t) \quad (9)$$

Equations 8 and 9 are the DC motor model state equations, where R, k_T, k_b, I_L and L are known constants of the motor or known properties of the circuit; $v_o(t)$ is the input and $i(t)$ & $\omega(t)$ are the outputs. This can be modelled in *Simulink* as seen below in figure 5. The equations and model assume that the motor is frictionless, which is not the case in actuality, however it is considered as such for this application. From this model, the torque at the shaft can be modelled depending on the voltage input to the model, and actuation of the steering of a bicycle or motorcycle can be built into this.

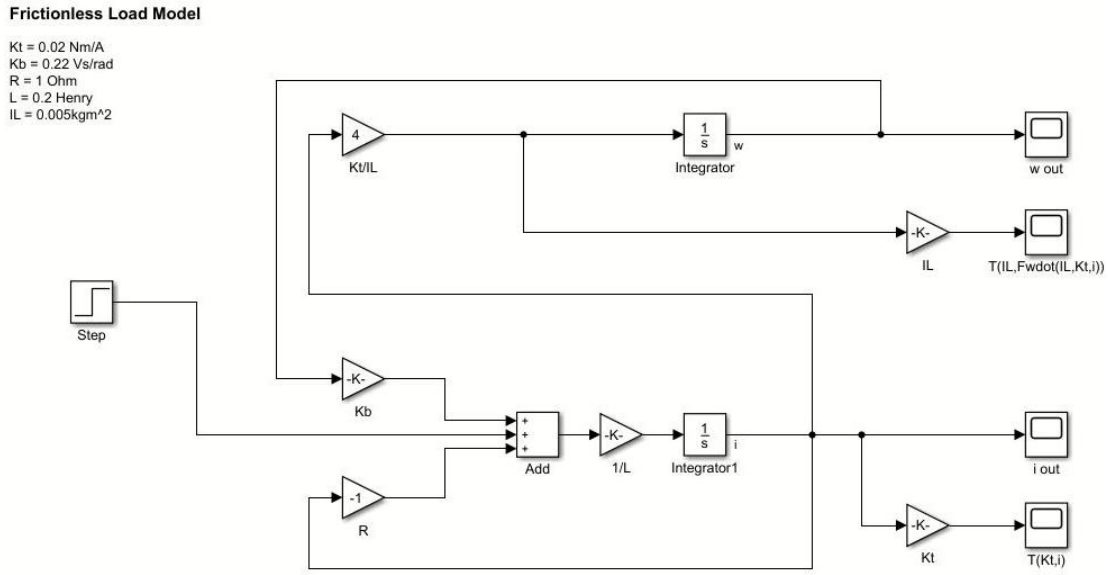

Figure 5 – The *Simulink* model of the frictionless DC motor, built from equations 8 & 9, including constants from a selected motor as an example.

3.2 Actuated Steering Dynamics and Modelling

Before the integration of the DC motor model and the motorcycle model can take place, there is an intermediary step. For actuated steering there must be a mechanism between the driving device and the motion being driven i.e. there must be a transfer of torque produced at motor shaft to the steerer of the cycle. To transfer torque across two parallel shafts, this can come in various forms such as belt drives and gear mechanisms. Since some past work has involved helical gears of a certain ratio, actuated steering for this application is modelled as such, but it could be modelled in other ways, considering different drivetrain techniques, using a similar technique than that shown here.

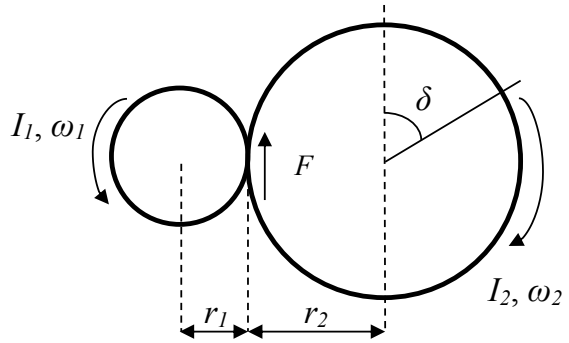

I – inertia

r – gear radius

δ – angle

ω – angular speed $(\omega_2 \equiv \dot{\delta})$

Figure 6 – A free body diagram that represents a helical gear assembly between the motor shaft and the steerer, from which the steering dynamics can be derived and modelled.

Figure 6 simplifies the driving mechanisms between the motor and the steerer and allows the dynamics of such a system to be derived and modelled before being merged with DC motor model and then the motorcycle model. In the model above, the smaller gear, gear 1, is the driving gear whose properties are referred to with the appropriate subscripts. The larger one, gear 2, is the driven gear, attached to the steerer of the vehicle, which too has its respective subscripts. Equations 10 and 11 below relate the mechanics of one another to the mechanics of the objects they are attached to.

$$I_1 \frac{d\omega_1}{dt} = ik_t - Fr_1 \quad (10)$$

$$I_2 \frac{d\omega_1}{dt} = Fr_2 - T_{GND} \quad (11)$$

Equation 10 relates the angular speed of the motor shaft to the balance of the torques acting on it. The torque produced by the motor, ik_t, is resisted by the force, F, and is equal to the moment of inertia of the shaft, I, multiplied by the angular speed, ω.

Similarly, equation 11 relates the angular speed of the steerer shaft to the balance of the torques acting on it. This time, however, the angular rate of the steerer depends on the moment of inertia of the steering column itself, the torques from the mechanism and the resistive torque from the front tyre against the ground, T_{GND}.

The resistive torques from the ground can be modelled as a function of the steering angle, δ, due to the caster effect of the front wheel and tyre forces that correct the heading of the front wheel. The greater the steering angle, the greater the resistive torque.

Once more, some manipulation allows them to be expressing in a particular form that allows the steering mechanism to be modelled alongside the DC motor. The process is as follows:

Rearranging equation 10 gives:

$$F = \frac{1}{r_1}\left(ik_t - I_1 \frac{d\omega_1}{dt}\right) \quad (10a)$$

Substituting equation 10a into equation 11 gives:

$$I_2 \frac{d\omega_2}{dt} = \frac{r_2}{r_1}\left(ik_t - I_1 \frac{d\omega_1}{dt}\right) - T_{GND} \quad (11a)$$

which can be expanded to give equation 11b below and can then be rearranged to put the differential terms on one side, as follows:

$$I_2 \frac{d\omega_2}{dt} = \frac{r_2}{r_1} ik_t - I_1 \frac{d\omega_1}{dt}\frac{r_2}{r_1} - T_{GND} \quad (11b)$$

$$I_1 \frac{d\omega_1}{dt}\frac{r_2}{r_1} + I_2 \frac{d\omega_2}{dt} = \frac{r_2}{r_1} ik_t - T_{GND} \quad (11c)$$

Knowing the relationship between the gear ratio and the angular rates, given by equation 12, equation 11c can be rewritten as follows:

$$\frac{d\omega_1}{dt} = \frac{d\omega_2}{dt}\frac{r_2}{r_1} \quad (12)$$

$$I_1 \frac{d\omega_2}{dt}\frac{r_2}{r_1}\frac{r_2}{r_1} + I_2 \frac{d\omega_2}{dt} = \frac{r_2}{r_1} ik_t - T_{GND} \quad (11d)$$

This can be simplified, giving the final form shown below in equation 13:

$$\left(I_1 \left(\frac{r_2}{r_1}\right)^2 + I_2\right)\frac{d\omega_2}{dt} = \frac{r_2}{r_1} ik_t - T_{GND} \quad (13)$$

To merge this model with that of the DC motor, a variant of equation 6 is recalled and manipulated using the angular rate relationship, from equation 12, forming the function in equation 14:

$$v_0 = iR + L\frac{di}{dt} + k_T\omega_1 \qquad (6c)$$

$$v_0 = iR + L\frac{di}{dt} + k_T\frac{d\omega_2}{dt}\frac{r_2}{r_1} \qquad (14)$$

Just as before for the DC motor, equations 13 and 14 can be used together to form another model, such as the one in Figure 7, that solves the equations for the angular rate of the steering response, ω_2, from the voltage input of the motor. For simplification, some of the constants used in the governing equations have been abbreviated using the following relationships:

$$A = I_1\left(\frac{r_2}{r_1}\right)^2 + I_2 \qquad (15)$$

$$GR = \frac{r_2}{r_1} \qquad (16)$$

Best practices for the process of building the model from equations such as these involves use of an initialisation file to define the constants, such as those in equation 15 and 16, and systematically going through the terms of the governing expressions, equations 13 and 14 in this case. Figure 7 also highlights the advantage of computational modelling, that is the ability to monitor a number of outputs at each stage of the transmission process over time, such as the torques, steering angles, voltage supply and current. Furthermore, the parameters of the model can be changed to test how the model responds to different types or combinations of motors as well as transmission mechanisms or gear ratios.

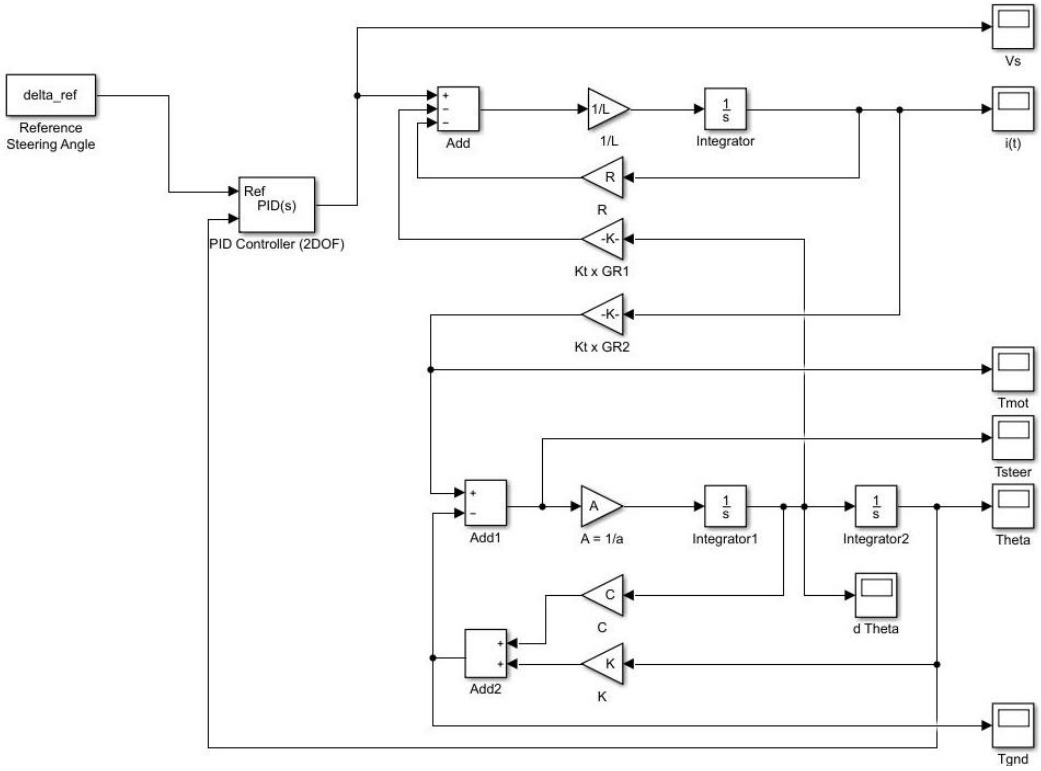

Figure 7 – Model of the DC motor and steering transmission mechanism. Many outputs from various stages of the process can be obtained from this model. As an exercise, this model includes a PID control term to achieve a desired steering angle from a voltage input.

3.3 Integration of the DC Motor & Motorcycle Models

Before getting into the integration process, an introduction to the motorcycle model, that has been repeatedly mentioned up to now, must be formally made. This model is a pre-existing one, normally used by final year MEng vehicle dynamics students, and supplied to the author by his supervisor for use in this project. The model uses the PID controller to control a parameterised motorcycle in a steady turn. Motorcycle dynamics are comparable to those of a bicycle due to their in-line, two-wheeled configurations and varying in only a limited number of ways, such as their mass, power, suspension characteristics and so on. The differences are not considered here as they do not apply to the integration process.

Figure 8 illustrates how the models have been merged. Since the steering dynamics are already included in the motorcycle model to an extent, it was the motor-derived components of the model in figure 7 that needed to be inserted, which can be seen on the right-hand side of the lower section of figure 8. The first connection made to the transplanted model is the steering angle, fed from the motorcycle to the motor, as the input to this section of the model. The second is the steering torque from the motor to the steerer of the motorcycle via the transmission mechanism. The final connection is the voltage input from the PID controller. Thus, steering toque to control the vehicle is obtained as a function of the voltage supplied.

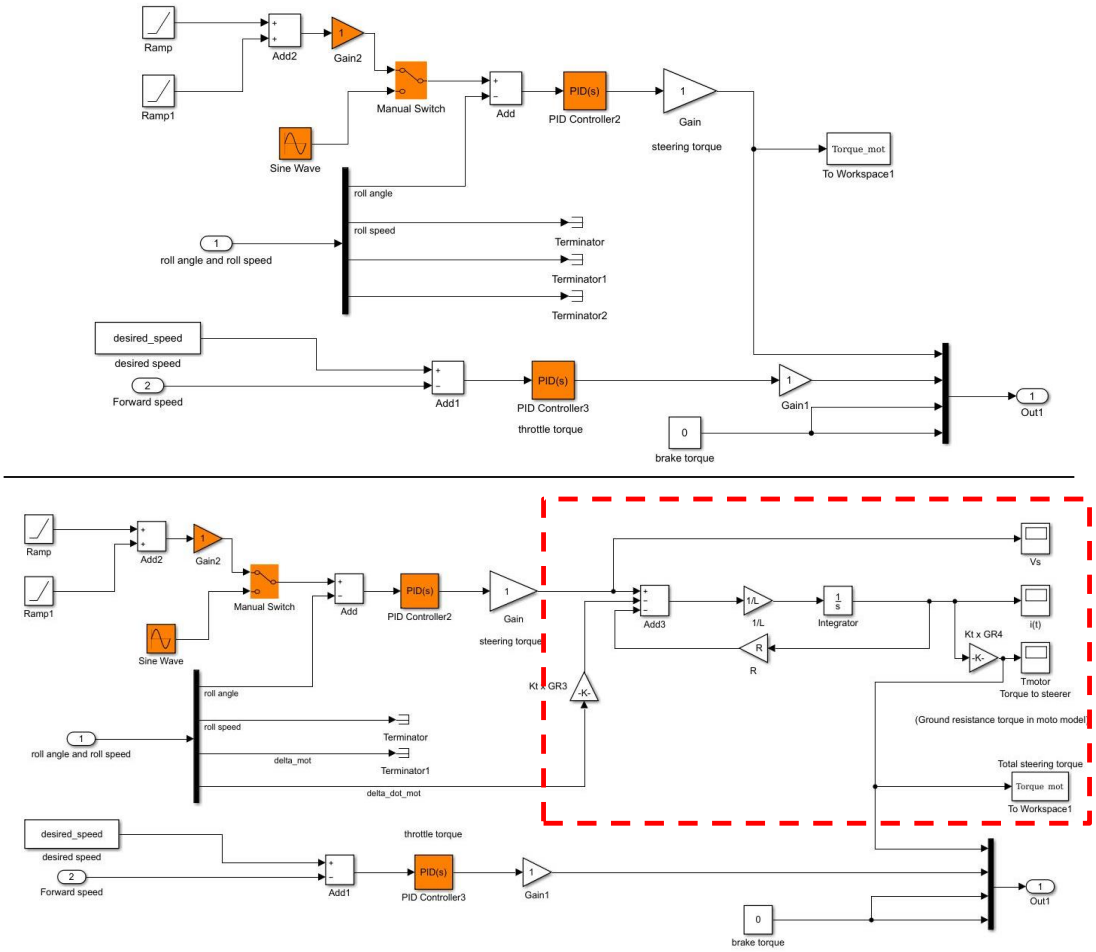

Figure 8 – Demonstration of the integration of the model from figure 7 with the motorcycle model. The model prior to the addition of the DC motor is shown in the top image, whilst the lower one shows the how the two are integrated.

3.4 Initialisation, Parameterisation & Tuning

Initialisation is the process of defining the constants and setting up the state space representation of the model. In addition to adapting the model, the original initialisation script for the motorcycle model needed adapting to accommodate the transplanted model of the DC motor as its steering actuator. Firstly, the motor and torque transmission properties need to be defined as constants for that segment to function as intended, so the properties of a real motor were chosen as an example and are defined in Table 1 below. Secondly, the moments of inertia of the motorcycles steering column needed to be redefined to reflect the new influences of the gear ratio and the motor on it, which was a case of adding the required constants to the pre-existing values of the initialisation script.

Property	**Value [Unit]**
Motor Voltage, V_{in}	12V DC
Zero Load Speed, ω_0	20,500 RPM*
Maximum Efficiency Torque, T_0	4500 g-cm*
Torque Constant, k_t	0.0056 N.m/A
Inductance, L	0.0015 H
Resistance, R	0.152 Ω
Motor Inertia, I_1	0.00025 kg.m
Motor Gear Radius, r_1	40 mm
Steerer Gear Radius, r_2	80 mm

Table 1 – DC motor model initialisation constants and transmission gear radii. Asterisk represents units requiring conversion to SI, a task that is completed by the initialisation script.

Following this integration and parameterisation processes, the motorcycle model functioned perfectly with the new steering control method and the response could be tuned, just as before, using the PID controller. Thus, the motorcycle was still being controlled using steering torque, but now using a DC motor as the actuator and as function of the voltage supply.

Another objective of this modelling process was to re-parameterise the motorcycle parameters, such as the suspension and mass mentioned before, to turn it into a bicycle. After that, further tuning could take place that would allow the new bicycle model to be controlled by the DC motor in the same way as for the motorcycle. This re-parameterisation process is a seemingly straightforward one that was also a milestone for this project, but it has not been attained in the time available and so it remains an outstanding task for further work in addition to the other recommendations made later in this report.

4 Bicycle Instrumentation Module

4.1 Specification

To balance a vehicle or system, the controller must be able to perceive some key variables that describe the state of the system. Perception of these variables at a point in time allows an informed control input to be applied, preserving the stability of the system. Knowledge of these variables is important for effective control and is known as state estimation. For a bicycle, these variables would be its forward velocity and its attitude, providing a picture of the acceleration of the of the centre of mass and its position over the contact points.

When humans ride bicycles, they are simultaneously the state estimation and the control systems as a result of their natural equilibrioception and biomechanical abilities evolved over centuries. To replicate this human skill artificially, an electronic and computational state estimation system that measures and deduces the physical position or attitude of the system at a suitable frequency is required. Such abilities can be obtained to some degree using a device consisting of (MEMS) sensor technologies, for example accelerometers and gyroscopes for this application, with the appropriate computational abilities which, in combination, can be likened to the human's vestibular sensory system that aids equilibrioception, or balance.

In addition to instrumenting the bicycle for attitude estimation, the device would have to measure or compute the vehicle's velocity, data not typically available to casual bicycle users, which is an important component of the small roll angle estimator, described later in section 4.3.1. Finally, the device would have to comprehensively record the measurements to a storage device in order to access and analyse them after any tests. To achieve autonomous steering control, biomechanical systems are replicated using a DC motor as the actuator delivering the steering torque but, whilst this has been covered in the previous section on computational modelling of such an actuation method, practical attempts at this have not been carried out.

4.2 Design

The process of obtaining a reliable estimate of the roll angle begins with installing the appropriate, adequate instrumentation which, for the purposes of this work, came in the form of two GY-521 3-axis accelerometer and gyroscope modules equipped with the MPU-6050 sensor chip. This device enables the angular rates and accelerations of the bicycle to be measured in three axes and six degrees of freedom which can then be used to compute a reliable roll angle estimation. Enabled by the two I2C addresses of an Arduino microcontroller, two of these sensor modules are included for both redundancy in the event of failure and for greater reliability of the measurements taken. This precaution would pay off when it came to practical testing of the assembled device in the field.

Another instrument, a Hall effect sensor, is included to detect the influence of the magnetic field of a magnet attached to a spoke on the rear wheel. To this end, the device is effectively a wheel speed sensor, measuring the time between interruptions, to calculate the angular rate, and using it with the radius of the wheel in equation 5 to calculate the speed of the vehicle. The Hall effect sensor also served as an odometer for the vehicle, counting the number of wheel revolutions and calculating an approximation of the distance travelled by the bicycle which would later become a useful metric for the performance assessment of this feature.

The complete sensor module, a circuit diagram for which is shown in figure 9, can accommodate an SD card, providing ample storage space for real time recording of the measurements as well as convenient removal and transfer of the data to another device for post processing and analysis. For optimum functionality and ease of use, the device employs the use

of a status LED to indicate whether or not the device is operating correctly, a switch to conveniently begin & end recording, a large capacity 9V power supply, and an electrolytic decoupling capacitor across the supply to act as a reservoir cap and keep the supply rail stable.

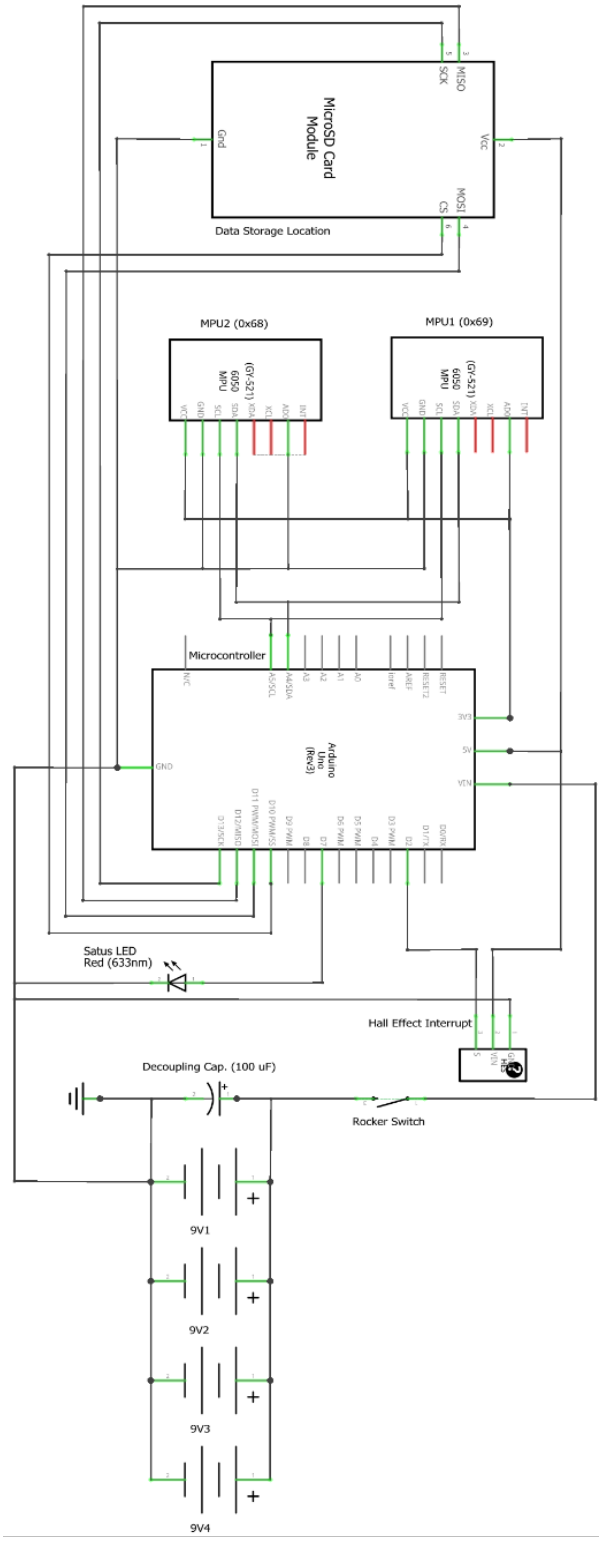

Figure 9 – Circuit schematic of the electronics required for the instrumentation of a bicycle for roll angle estimation and data storage, showing how each component required for reliable estimation of the roll angle is connected to the controller as well as any other components required for ease of use of the device. Information on the assembled device and an assessment of its performance can be found in the sections that follow.

4.3 Assembly

The assembly process encompasses both the integration of the hardware components as well as the creation and implementation of the software required for the device to function as intended. These two distinct, but overlapping, parts of the process ran alongside one another; the hardware assembly for a particular function was prototyped on a solderless breadboard and code to perform that function was tested, as a separate module, before moving onto another feature. For example: first the Hall effect sensor was set up and a C code program was written and tested to ensure that the speed and distance calculation functions were working as intended before repeating the process with the two IMU sensors and the SD card module.

Once each module was functioning correctly, all the pieces of code, one for each device or respective feature, were compiled as a single program and tested on a prototype assembly of all the components as a complete device. After completing this, a second prototype of the device was rebuilt using more permanent methods. Each connection to the Hall effect sensor was soldered to a 0.65-metre long wire, giving it the necessary length to extend to the rear of the bicycle, which were in turn plaited and sealed in heat shrink wrap to form a strong, well insulated cable to protect it in its operating environment, as well as being aesthetically pleasing.

An unbranded Arduino Uno variant was sourced and used as the controller due to the demand for additional 3.3-volt, 5-volt and ground pins, which this variant was able to supply where the Arduino could not. Four 9-volt battery connectors were soldered together to allow tidy and convenient connection to the power source. It was at this stage that the status LED, the decoupling capacitor and the switch were incorporated into the design for greater functionality and ease of use without the need for any significant alterations to the circuitry or to the code.

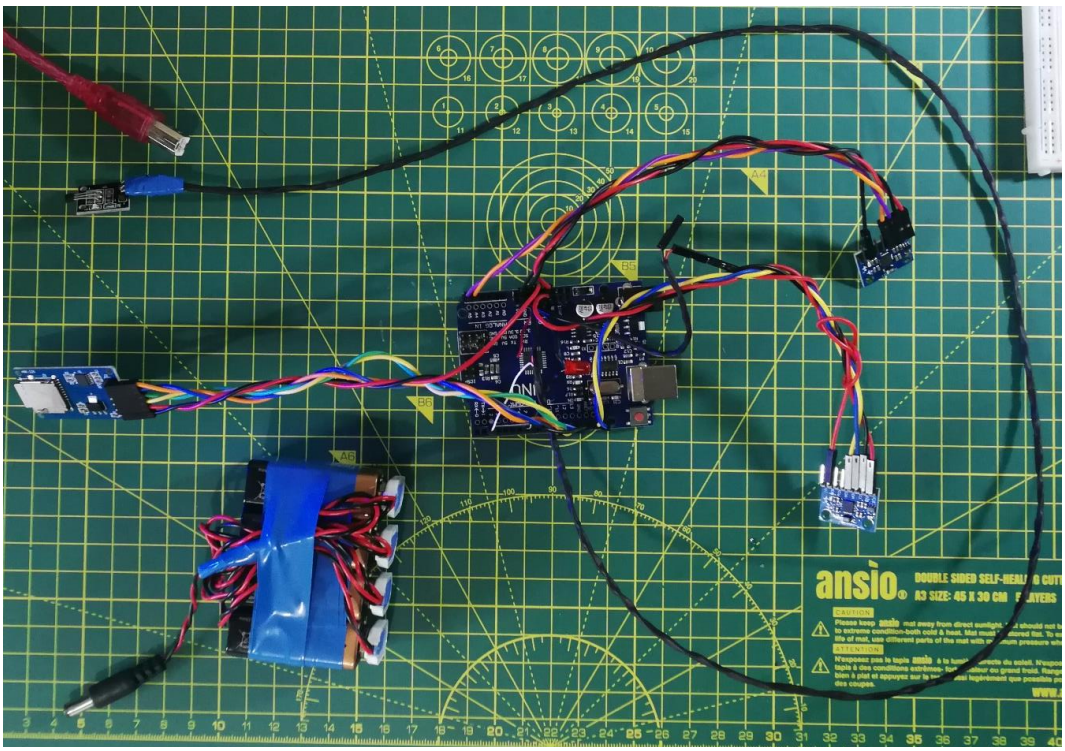

Figure 10 – The completed assembly of the instrumentation electronics, photographed here, prior to being installed in the housing container and fitted to the test bicycle. The long, black lead is the connection to the Hall effect sensor, the two IMUs can be seen on the right, the SD card module is to the left above the 9V power supply and the microcontroller is in the centre.

4.4 Installation & Testing

4.4.1 Installation

From the author's experience of the iterative nature of the prototyping process gained through previous projects and industrial experience, the module unit needed to be accessible throughout and so a complex, permanent fixture to the test vehicle was neither necessary nor advantageous. From a safety standpoint, the electronics and any other external parts had to be self-contained and fastened without impeding the rider or negatively affecting the handling qualities of the bicycle for the duration of any dynamic field tests and the associated conditions.

The electronics for the sensor module were housed in their entirety within a repurposed sports drink bottle to contain and protect the components in a compact, unobtrusive manner for the safety of the rider when using the bicycle. The bottle was designed to fit securely in standard cycling bottle cages, permitting ease of access to the unit for removal and reinstallation of both the SD card and the whole unit itself, as well as securing it to the frame of the bicycle for recording measurements. In addition to the main unit, a couple of peripheral components associated with the operation of the wheel speed sensor feature needed to be attached to the bicycle.

Figure 11 – Photographs of the fully installed sensor unit. The IMUs are aligned parallel to seat tube of the bicycle.

The first of these was a spoke magnet, securely attached to a rear wheel spoke using a threaded and toothed fastener. The magnet was as small and as light as required, minimising any impact it may have on the handling of the bike resulting from the offset centre of mass of the rotation wheel. Secondly, the single cable connecting the unit to the Hall effect sensor was safely fastened to the frame of the bicycle, out of the way of the drivetrain and the rider's legs. The Hall effect sensor was attached securely some distance further along the frame, to the chain stay of the bicycle, in proximity of the rear wheel spokes and well within range of the magnetic effect of the spoke magnet.

Within the improvised housing, the IMUs were glued securely to the inside and the container was placed in the bottle cage such that they were aligned parallel to the seat tube of the bicycle. Furthermore, they were placed as close to the frame mounting bolts as possible to try and reduce the effects of vibration of the whole assembly on the measurements taken during testing, assuming that the amplitude of the vibrations would be smallest at this location. No problems were encountered during the installation of the device. A very valuable quality of the complete device was that all parts required for the unit to function as intended could be added or removed quickly without damage to the bicycle whatsoever, enabling ease of operation and minimising the risk of additional costs or delays due to damage.

4.4.2 Bias Test

Following the installation of the sensor module on the test bike, two static tests were conducted to assess the performance of the system and identify any early flaws, particularly in the two IMU sensors. The first of these was a bias test to try to identify if either of them had any biases in their readings. With the instrumentation equipment in place and recording, the bicycle was placed in a straight & level position and left alone for a duration of approximately 15 minutes gathering data in a motionless state. In a motionless, straight and level state, the author expected to find zero readings in all gyroscope axes as well as the X and Y accelerometer axes followed by a measurement approximately equal to *g* (gravitational acceleration on Earth) in the Z-axis of the body frame of reference.

Table 2 below shows the properties of the sensors extracted from the data from this test. The performance of one of the IMUs (GY-521-1) appears to be better than the other such that the measurements from the second IMU can be regarded as slightly less reliable than those from the first. In the orientation test that follows, this superiority becomes starker. The biases of the sensors, and the gyroscopes in particular, are useful to know for the implementation of the Kalman filter as it is one of the components of the model used, whilst the standard deviation is useful for the assessment of this filter algorithm. Both of these processes are covered in depth in the next section.

The reader will notice that the acceleration readings in the Z & Y axes do not record a mean of zero or ~9.81 m/s respectively as they should. This was the early sign suggesting there was a misalignment of the IMUs with the bicycle's body frame of reference, which was confirmed by the data from the orientation test that followed this. Some corrected mean measurements are included in brackets for the appropriate vectors but the process of correcting the data is covered in the context of the orientation test later in this section. Plots of both the raw and corrected data from this test are available in the Document Notes section of the appendix.

IMU No.	Sensor	Sensor Axis	Mean (Bias), $\bar{x}$ [m/s]	Variance, σ^2 [(m/s)^2]	Standard Dev., σ [m/s]
GY-521-1	Accelerometer	X	0.203	0.001	0.036
		Y	9.426 (9.808)	0.001	0.033
		Z	2.714 (-0.075)	0.002	0.046
	Gyroscope	X	-0.080	1.47×10^{-6}	0.001
		Y	-0.010	1.01×10^{-6}	0.001
		Z	-0.008	1.33×10^{-5}	0.004
GY-521-2	Accelerometer	X	-0.307	0.02	0.039
		Y	9.384 (9.495)	0.01	0.036
		Z	1.752 (-0.986)	0.03	0.050
	Gyroscope	X	-0.018	4.60×10^{-5}	0.007
		Y	-0.052	4.58×10^{-5}	0.007
		Z	0.074	4.58×10^{-5}	0.007

Table 2 – Properties of each GY-521 IMU following the static bias test. The mean is effectively the bias of the sensor since the measurement truth for each axis should be zero.

4.4.3 Orientation Test

After the bias test, an orientation test was conducted to relate the measurements recorded by the sensors to the actual motions of the bicycle as well as helping to visualise how the reference frames of the sensor were aligned with those of the global and body frames. This was achieved by isolating the bicycle in each of the six degrees of freedom being measured and matching the 'choreographed' motions of the bicycle from the test to the measurements taken in time. Table 3 shows how the measurements relate to the actual movement of the bicycle and sensor axes align with the reference Euler axes defined at the beginning of section 2.

Measurement	Sensor Axis	Measurement Sign		Equivalent Body Axis
		Positive	Negative	
Acceleration	X	Lateral acceleration to the left	Lateral acceleration to the right	Y
	Y	Vertical acceleration upwards	Vertical acceleration downwards	Z
	Z	Acceleration in direction of travel	Deceleration in direction of travel	X
Angular Rate	X	Downward pitching motion / Declination	Upwards pitching motion / Inclination	Y
	Y	Yawing motion anticlockwise/to the left	Yawing motion clockwise/to the right	Z
	Z	Rolling motion clockwise/to the right	Rolling motion anticlockwise/to the left	X

Table 3 – Qualitative definitions of the measurements taken, describing the motion they correspond to in practice. They are defined relative to the rider of the bicycle and the motions they experience. The equivalent Euler axis of each sensor axis is also identified.

To summarise the events of the angular rate orientation test: the first 75 seconds comprised of rolling motions, the next 25 seconds consisted of upward pitching motions and the final 50 seconds of yawing motions. Analysis of the data from the orientation test revealed a misalignment error and, more importantly, its consequences on the measurements properly for the first time. Assuming the IMUs were perfectly aligned with the body frame of reference of the bicycle, one would expect the data to show the yaw rate to vary in the final 50 seconds *exclusively*. Figure 12 shows that there are significant components of yaw rate measured in the rolling period of the test, which confirms that there is significant misalignment of the IMUs once installed on the bicycle and hence, an error in the measurements for the yaw rate. Figure 12 only shows measurements for the Y-axis measurements for brevity and clarity; however, it should be noted that the reverse is also true, there is evidence of undesirable roll rate components in the measurements taken during the yawing section of the orientation test.

This error is the result of an oversight in the design: the seat tube of the bicycle frame, upon which the device is installed, is offset from the vertical, meaning that even if the IMUs are installed perfectly vertically within the housing, an unlikely feat in itself, they will become misaligned once installed on the bicycle. Fortunately, it is possible to compensate for a misalignment error such as this if the angle by which it is offset is known, which it is. The manufacturer of the test bicycle lists the seat tube angle as 73.5 degrees from the horizontal,[26] or 16.5 degrees from the vertical.

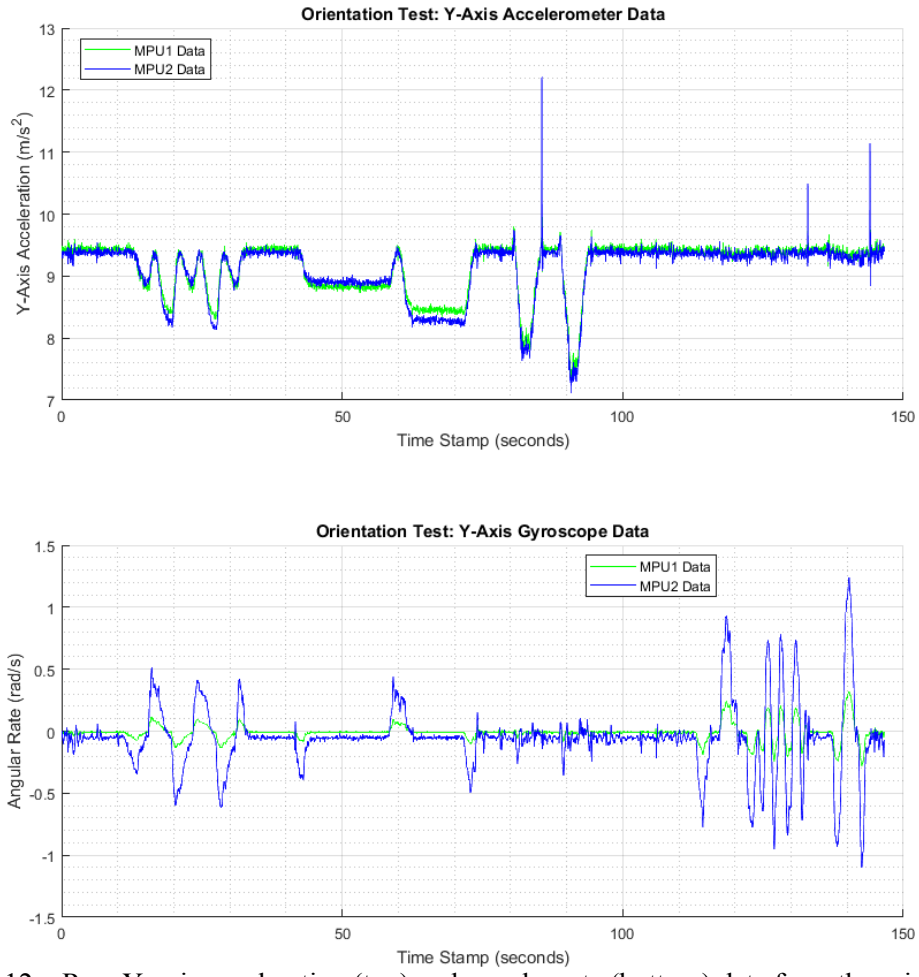

Figure 12 – Raw Y-axis acceleration (top) and angular rate (bottom) data from the orientation test. A noticeable component of the rolling motion is seen the yaw rate measurements in the first 50 seconds of the test due to the misalignment of the IMUs in the body's inertial frame. The reader is reminded that the Y-axis of the IMUs is approximately oriented in the direction of the Z-axis of the body frame of reference.

The actual misalignment angle may have other small contributions, such as from the fabrication of the device, the installation within the bottle cage, the fitment of the bottle cage to the frame and the addition of the wheels to the bicycle. Neglecting any of these contributions to the seat tube angle, the misalignment can be assumed to be a rotation about the X-axis of the IMU reference system (Y-axis in the body reference frame), a correction for which is given below.

$$\omega_c = [R_\varepsilon]^{-1}\, G_m \qquad (17)$$

The error can be corrected using equation 17 where β is the seat tube angle, R_β is the transformation matrix, G_m is a matrix containing the misaligned gyroscopic measurements of each axis and ω_c is a matrix containing the corrected angular rates in each axis, also in vector form.

$$R_\beta = \begin{bmatrix} 1 & 0 & 0 \\ 0 & \cos\beta & -\sin\beta \\ 0 & \sin\beta & \cos\beta \end{bmatrix}, \quad G_m = \begin{bmatrix} G_x \\ G_y \\ G_z \end{bmatrix}, \quad \omega_c = \begin{bmatrix} \omega_x \\ \omega_y \\ \omega_z \end{bmatrix}$$

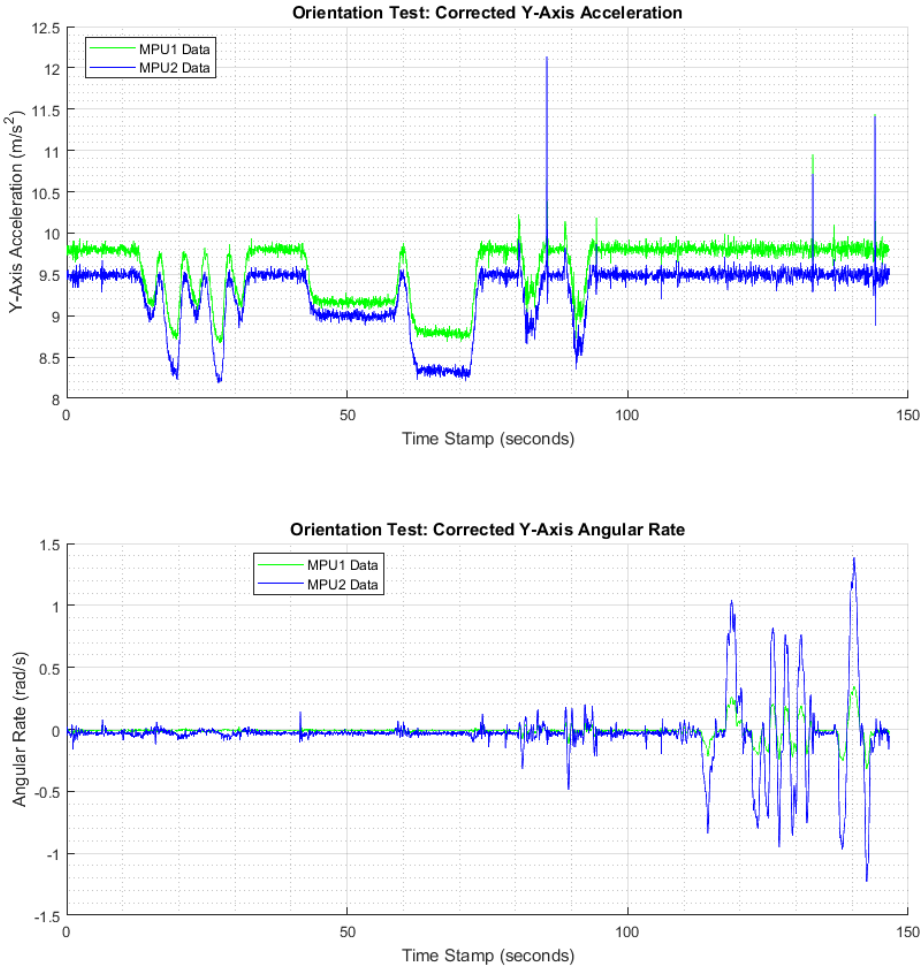

Figure 13 – Corrected Y-axis acceleration (top) and angular rate (bottom) data from the orientation test. Notice how the correction applied has removed a great deal of the roll rate component from the yaw rate measurements in the first 50 seconds of the test.

The same corrective calculation can be applied to the acceleration measurement vectors which also suffer from the same misalignment error as those of the gyroscopes. An example of outcome of applying the correction can be seen in figure 13 where absolute yaw rate is restored to its full magnitude, the influence of the roll rate is acceptably redacted from the measurements, and vice versa. Since the angular rates are all used in the subsequent roll angle estimation calculations, it is imperative that the measurements are as reliable as possible.

Figure 13, and Table 3, show that the acceleration measurements are also favourably corrected, causing the vertical acceleration magnitudes to be closer to the expected value of ~9.81 m/s^2 and approximately zero in the other directions. For the reader's reference, plots comparing all measurements made during this test and the results of the corresponding corrections are included in the appendix under the heading relevant to this section. With hindsight, such an error was predictable, and preventable using techniques discussed later, since there exist no perfectly vertical or horizontal tube on the frame geometry of a modern bicycle. Given the author's familiarity with bicycles, this ought to have occurred to him, yet it was still overlooked.

4.4.4 Test Errors & Reliability

The testing was conducted after installation of the sensor module as that would be its operating environment. The objective of this approach was to have fewer problems later in the process, compared to conducting the tests on the module prior to installation or in isolation. It was imperative that errors were minimised as far as possible in the bias test to have the best chance at accurately identifying any zero errors or other problems in the sensors' measurements. This could be done by ensuring that the bicycle was, and remained, in a straight and level position for the duration of the test. Three actions were taken to achieve this.

Firstly, by using a spirit level, the wheelbase and contact points of the bicycle could be made to span a suitably level patch of ground. Secondly, the bicycle was placed stably against a wall with the frame aligned as vertically as possible, using a plumb line for reference. In doing so, sources of error could be minimised, and any that remained could be attributed to the assembly of the electronics within the housing unit, the installation of the unit on the bicycle or the errors in the sensors themselves. Finally, by conducting the test over a long duration relative to the measurement period of the datalogger, reliable estimations of a mean bias could be made and any longer-term drift in the measurements would be identifiable.

Errors in the orientation test were less important since, as the name of the test might suggest, its purpose was to allow the author to identify the sensors' frame of reference with respect to that of the bicycle. However, some precautions were taken to ensure that the bicycle was free to rotate in a single degree of freedom and constrained in the other two. Such precautions included suspending the bicycle with a rope to conduct the yawing and pitching motions, ensuring that any motions were consistently steady and that the bicycle was moved through approximately the same angle in each manoeuvre.

With additional resources, a robotic test rig would have been ideal to conduct these tests with greater traceability and repeatability, for the wheel speed sensor especially, as is done professionally when testing reliability of comparable assemblies. Without such resources, these relatively primitive tests were adequate for determining the characteristics of the sensor unit and the subsequent reliability of the measurements taken.

4.5 Improvements & Modifications

The static tests contributed to the identification of two critical flaws in the sensor measurements which have been covered thoroughly in in section 4.4.3. Fortunately, through some foresight and further work, both of these could be corrected or compensated for in post process but that does not mean improvements to the design or installation of the module should be neglected and, as such, this section is dedicated to the author's suggestions in this regard.

The misalignment error between the frames of reference of the sensors and the bicycle, caused by the chosen mounting method and the angle of the mounting location, is undoubtedly the first and most important issue to address. Whilst this source of error was corrected in post processing of the data, a practical remedy to this is a relatively straightforward one and avoids the complexity of an additional corrective calculation. A simple wedged shim to offset the seat tube angle of the bicycle would do a reasonable job of correcting the error but the ideal approach would be to fabricate a bespoke housing unit with a specific mounting bracket, serving as both a container for the electronics and a robust mounting point that offsets the misalignment angle. This is a more advanced solution but, with modern CAD and access to 3D printers, a relatively straightforward and highly effective one. This would eliminate the large-scale misalignment angle from the bicycle's geometry, but such an error is perhaps inevitable and likely to persist on a smaller scale regardless of where the fixing points of the sensors are.

Furthermore, a static test prior to complete assembly and installation of the sensor module on the bicycle is recommended to identify the sensor properties and biases as an investigation into their reliability and accuracy, particularly in each axis. Such a test could also inform decisions on ways to orientate the sensors with respect to aligning their frames of reference with that of the bicycle for improved accuracy and precision of the measurements.

Other suggestions for improvements or modifications, identified following the field tests, are related to two sources: the effects of rider movement and of harsh road vibrations experienced during the test. It is impossible to discount the possibility that the rider may have inadvertently influenced the measurements taken through conscious or subconscious body lean when and through any secondary movements resulting from pedalling motions when propelling the bicycle. Options to minimise this include repeating the test using an electric bicycle and a rider under instruction to remain motionless at all times when conducting the test, thereby reducing the body movements as well as eliminating the need for pedalling, and any subsequent secondary motions.

The test vehicle was a fully rigid road bicycle, the kind designed for speed over the relatively smooth surface of modern paved road and therefore offering very little in the way of compliance and damping of vibrations from the terrain. Even the pneumatic tyres, which can deform, are relatively highly pressurised to reduce this. As such, the effect of such vibrations on the measurements might be to increase the amount of noise in them directly or, to a lesser extent, cause displacements that might add further noise indirectly. Using wider tyres at lower pressure and a partially or fully suspended bicycle for the test is likely to help a great deal with road vibrations directly. Ensuring that the sensors are securely attached as close to the frame as possible will also help to minimise the more indirect effects.

One final suggestion would be to take steps to improve the baud rate of the measurements taken. The author encountered memory and stability issues with the program running on the device when a recording rate any higher than 25 Hertz was selected. Improved computing resources could allow for higher measurement rates, possibly correlating to a more accurate estimation of the state of the bicycle as well as additional capacity for other capabilities of the control system.

5 Data Processing & Bicycle Roll Angle Estimation

5.1 Field Testing & Data Collection

Following the static tests, field tests were conducted to gather measurements in a real-world environment. The field tests consisted of the author riding two laps of the Loughborough University campus whilst measurements were taken by the sensor module for the duration, which lasted a total of approximately 15 minutes. The duration and route taken for the test provided ample opportunity for suitable measurements to be taken and scenarios to be analysed afterwards, such as roundabouts for prolonged, steady turns to be performed and sections of straight, level road to ride on with 'zero' roll. The tests were uneventful, the device and all electronics functioned as intended, initially giving the author no reason to believe there are any problems with the measurements taken. Post-processing of the data, however, revealed some irregularities, beyond just the bias, in measurements from the second IMU (GY-521-2) at large angular rates. These are henceforth neglected in favour of the measurements from GY-521-1, which showed no such irregularities, examples of which can be seen from the data in figure 12.

5.2 Forward Speed from the Wheel Speed Sensor

5.2.1 Real Time Data

The forward velocity of the bicycle is calculated by the program of the device in real time using equation 5c, a variant of equation 5, that employs the wheel diameter rather than the wheel radius, the trivial derivation for which is given below.

$$V = -\omega_{wr} R_{wr} \qquad (5)$$

$$V = -\left(\frac{2\pi}{t_{wr}}\right)\left(\frac{D_{wr}}{2}\right) \qquad (5b)$$

$$V = -\frac{\pi}{t_{wr}} D_{wr} \qquad (5c)$$

The wheel diameter, D_{wr}, is the is sum of the diameter of the rim and two widths of the tyre. For a standard road bicycle as used in the test, the rim diameter is 622 millimetres and the tyre width was 25 millimetres, giving a wheel diameter of 0.672 metres. The time for one revolution of the wheel taken from the time between interrupts from the Hall effect sensor, acting as a Wheel Speed Sensor (WSS). For the odometer feature of this module, the distance travelled by the bicycle is calculated using the wheel circumference and a running total of the number of wheel revolutions, n_{wr}, as shown in equation below:

$$S = \pi D_{wr} n_{wr} \qquad (18)$$

Both calculations neglect the deformation of the pneumatic tyre which is small for a bicycle such as this since the tyre is inflated to a high pressure and its tread is very narrow.

5.2.2 Performance Assessment using a GPS-based Speed Calculation

To validate the velocity measurements made by the device installed on the bicycle, the test was also recorded using a GPS-enabled Garmin Edge 520 head unit that measured the speed of the bicycle as well as the distance travelled using GPS based methods. The exact measurements could not be extracted from the Garmin device, however, the bicycle's velocity profile from the test was able to be produced using third party tools and compared with the measurements, as seen in figure 14. To filter any noise in the calculation of the speed from the WSS, a half second moving average has been applied and is shown here. An average over half a second corresponds to an average over 13 separate measurements. Other metrics from the test, such as the total distance covered, maximum and average speed, are compared in Table 4.

	Distance Travelled [km]	Maximum Speed [km/h]	Average Speed [km/h]
Garmin Edge 520	8.05	49.6	31.8
Custom Device (WSS)	8.20	49.9	32.4

Table 4 – Comparison of some field test metrics recorded during the field testing by the two devices. Measurements from the WSS have been converted to be comparable.

GPS-based estimation of velocity has flaws of its own that mean it cannot be relied on as anything more than a very useful refence, such as the measurement frequency, signal delay, accuracy of the co-ordinate measurement as well as any averaging or other algorithms that might be used to reproduce the data shown here. Whilst that the GPS cannot be taken as the ground truth, given that the velocity measurements from the Garmin and the custom device are both very similar in both magnitude and profile, it is safe to assume beyond reasonable doubt that the velocity measurement from the WSS is reliable enough to be used in the estimation of the roll angle.

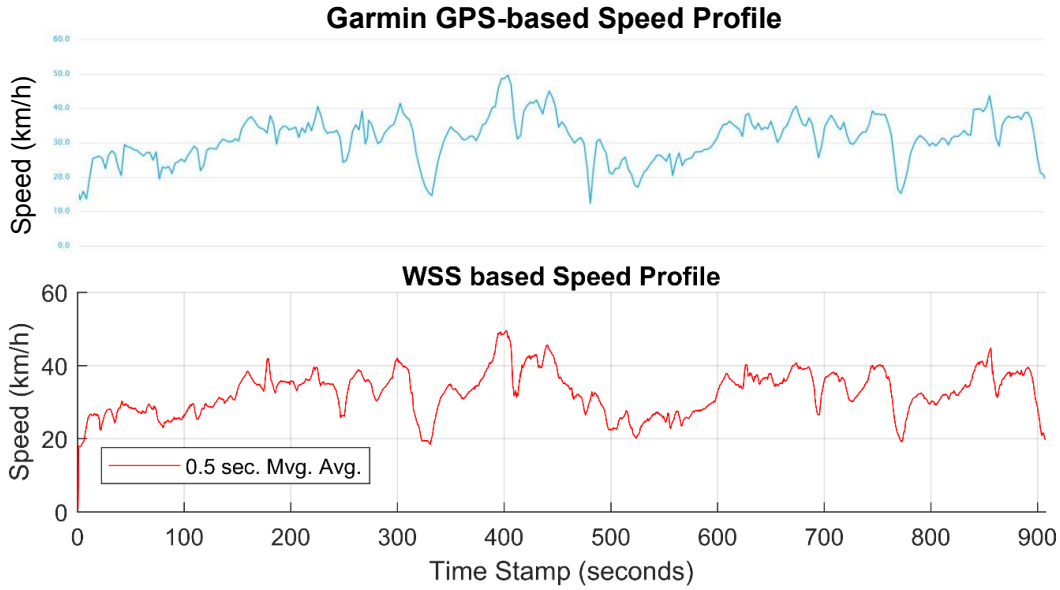

Figure 14 – Plot comparing the GPS and WSS measurements of velocity over the duration of the field test conducted on campus. Note the nearly identical profiles.

5.3 Early Roll Angle Estimation Methods from Raw Data

The supplementary calculations and algorithms, as a method of estimating the roll angle of a bicycle, put forward by *Sanjurjo et al.* 2019[20] were identified by the author as the optimal approach for the purposes of this work. They suggest a second, separate approximation for more extreme roll angles due to the fact that the calculation of the roll angle using the lateral dynamics equations can produce noisy approximations at large roll angles.[22] When used in combination, a reliable estimate of the roll angle can be obtained. Furthermore, they go so far as to validate their strategy favourably by experiment, demonstrating that their method gives a reliable estimation with impressive root mean square error of less than 2 degrees.[20] Angular terms used in calculations are in radians whereas the results are displayed in degrees for greater simplicity and conceptualisation for the readers. This process is covered in detail as follows.

5.3.1 Small Roll Angle Approximation, φ_d

The first approximation of the roll angle is calculated using the lateral dynamics equilibrium equation from the steady turn case covered in section 2. The yaw rate and vehicle velocity variant of the equation (reproduced below) is used to make the estimation when it is less than approximately 20 degrees from the vertical. This calculation is referred to as the small angle approximation.

$$\varphi_d = \tan^{-1}\left(\frac{V\dot{\psi}}{g}\right) \qquad (3)$$

The yaw rate in the global frame of reference is difficult to calculate or measure precisely, so for this calculation the angular rate measurement made by the Y-axis gyroscope is used as an estimation for this variable. The half-second moving average of velocity is used as the estimation for the velocity variable in this equation.

5.3.2 Large Roll Angle Approximation, φ_w

Given that the small roll angle approximation is prone to producing noisy approximations for the roll angle, a second estimation that uses the angular rates in the Y and Z axes and shown by equation 19, is employed for approximated larger roll angles of 20 degrees or above.

$$\varphi_\omega = \tan^{-1}\left(\frac{\dot{\theta}}{\dot{\psi}}\right) \qquad (19)$$

The equation above can be rearranged into the format shown by equation 20. They are mathematically equivalent and the new format below avoids computing errors caused by attempting to divide by zero in the event of such a measurement for the yaw rate.

$$\varphi_\omega = \mathrm{sgn}(\dot{\psi}) \cdot \sin^{-1}\left(\frac{\dot{\theta}}{\sqrt{\dot{\theta}^2+\dot{\psi}^2}}\right) \qquad (20)$$

Problems still occur with this function, however, in the rare event that *both* measurements for the pitch and yaw rates are zero readings. Ironically, this occurrence became reality for the author, who was baffled initially by a single event in a data pool of over 426,113 measurements but was able to correct it programmatically by assigning both measurements a small value, equal to 1×10^{-4}, and successfully able to avoid a mathematical error in all subsequent calculations.

5.4 Late Roll Angle Estimation

Late roll angle estimation, in this context, is the process of combining the results from the early roll angle estimations from earlier in this this section, the large and small approximations, to produce an even more filtered and refined estimation. There are two methods used in this process, the first is the use of a blending function to vary the weighting assigned to the small or large roll angle approximations, depending on the magnitude of the angle. This function is embedded within the second technique used in this process, a Kalman filter algorithm, to provide a virtual measurement to this algorithm which then computes the final estimation of the roll angle. This section walks through the implementation of this process and the results that are produced.

5.4.1 Use of a Blending Function for Virtual Roll Angle Measurement, φ_m

The two roll angle approximations from the earlier stage are weighted using a blending function which resembles the 1st order low-pass filter and is given by equation 21. The weighting is assigned by a co-efficient, *W*, given by equation 22, is a function of the most recent roll angle

estimation from the stochastic Kalman Filter, $\hat{\varphi}$, and a constant, $\bar{\varphi}$, that allows the co-efficient to be tuned.

$$\varphi_m = W\varphi_d + (1 - W)\varphi_\omega \quad (21)$$

$$W = \exp\left(-\frac{\hat{\varphi}^2}{\bar{\varphi}^2}\right) \quad (22)$$

$$\bar{\varphi}^2 = 0.05 \quad (23)$$

The influence assigned by the blending co-efficient, W, varies depending on the roll angle. As the magnitude of the estimation from the Kalman filter approaches ~20°, the co-efficient, W, decreases, reducing the influence of the small angle approximation component in the calculation, φ_d, and increasing it for the large roll angle component, φ_ω. The opposite is true when the Kalman estimation is small, the calculation relies more on the small angle component and less so on that of the large angle. This is demonstrated visually in figure 15. The result of the blending function is a virtual measurement of the roll angle that is fed into the Kalman Filter algorithm to compute a new estimation for the present time step.

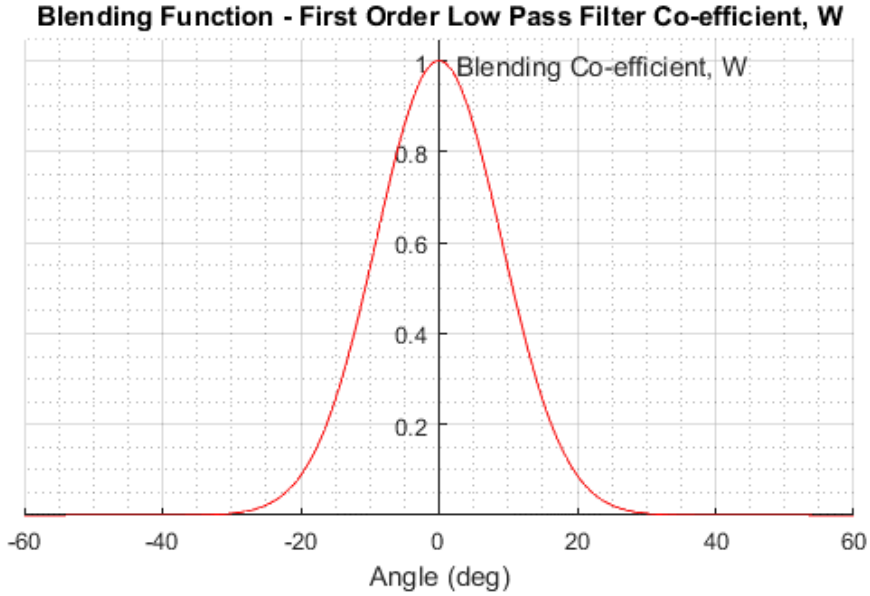

Figure 15 – Visual representation of the function that defines the blending co-efficient, W, and, hence, how it assigns a weighting to the large or small roll angle approximations using the blending function to produce a virtual measurement for the Kalman filter.

5.4.2 Use of a Kalman Filter for Final Roll Angle Estimation, $\hat{\varphi}$

The Kalman filter is powerful tool that uses system modelling and recursion to produce a reliable estimate of the state of a system measured in the presence of noise. Neither the theory nor the context of the Kalman filter are the subject of this work so, in the interests of brevity and relevance, the remainder of this section is limited exclusively to breaking down the steps of implementing the technique, proposed by *Sanjurjo et al.*,[20] to obtain the 'real time' roll angle estimation of a bicycle.

The Kalman filter stages are broken down and implemented in the format below. After the initial values are set, the recursive algorithm loops continually through steps 1-4 using the

sensor measurements and the roll angle approximation methods as the inputs. The subscripts *k* and *k – 1* indicate states or values at the present timestep and previous timestep respectively.

0. Initial values for the state, $\hat{x}_0$, and error covariance, P_0, are set and program starts.
1. a) A new prediction of the state, $\hat{x}_k^-$, and error covariance, P_k^- are made using the dynamic model and the specific equation respectively, as seen below:

$$\hat{x}_k^- = A\hat{x}_{k-1}^- + Bu_{k-1} \quad (24)$$

$$P_k^- = AP_{k-1}A^T + Q \quad (25)$$

   b) A new value for the blending function coefficient, W, is calculated using equation 22 followed by a new approximation of the roll angle using equation 21.
2. The Kalman gain, K_k, is calculated:

$$K_k = P_k^- H^T (HP_k^- H^T + R)^{-1} \quad (26)$$

3. An estimate, $\hat{x}_k$, is calculated from the input measurement, z_k, which in this case is the roll angle approximation, φ_m, from step 1.b), and fed back to step 1.a) as $\hat{x}_{k-1}^-$.

$$\hat{x}_k = \hat{x}_k^- + K_k(z_k - H\hat{x}_k^-) \quad (27)$$

4. The error covariance, P_k, is recalculated and fed back to step 1.a). as P_{k-1}.

$$P_k = P_k^- - K_k H P_k^- \quad (28)$$

The dynamic model used, given below in equation 29, is the one put forward in the literature, and uses the measurement from the roll rate sensor, $\dot{\varphi}$, and the bias of this sensor, $\hat{b}_x$:

$$\begin{bmatrix} \hat{\varphi} \\ \hat{b}_x \end{bmatrix}_k^- = \begin{bmatrix} 1 & -dt \\ 0 & 1 \end{bmatrix} \begin{bmatrix} \hat{\varphi} \\ \hat{b}_x \end{bmatrix}_{k-1}^+ + \begin{bmatrix} dt \\ 0 \end{bmatrix} \dot{\varphi}_{k-1} \quad (29)$$

where $\hat{\varphi}$ is the roll angle estimation and $\hat{b}_x$ is the bias of the gyroscope measuring the roll rate. The assumption of the sensor bias as constant is fair given that the static tests showed no evidence of drift in the angular rate measurements over time. The integration timestep, *dt*, is set to the time period between the roll rate measurements being taken which is approximately equal to 0.04 seconds for a measurement frequency of 25 Hertz.

Setting the state-to-measurement matrix, *H*, as equal to 1 produced extremely favourable results for the estimation of the roll angle. The covariance matrix of the plant noise, *Q*, is assigned as recommended by the literature but the covariance matrix measurement noise, *R*, is set to the covariance of the roll rate measurements from the static bias test.

$$H = 1 \quad (30)$$

$$Q = \begin{bmatrix} 5 \times 10^{-7} & 0 \\ 0 & 1 \times 10^{-8} \end{bmatrix} \quad (31)$$

$$R = 1.332 \times 10^{-5} \quad (32)$$

Limited computing resources prevented this algorithm from being included in the program running on the sensor module itself so it was done in post processing of the test data, however, this could be achieved in theory and the roll angle estimation could be computed in actual real time rather than 'offline.' The virtual measurements and roll angle estimations for the two occasions that the bicycle navigates a pair of roundabouts by the West Park entrance of campus (shown in figure 16 for readers unfamiliar with the area) are shown in figure 17. This period

of the field test is chosen for clarity and since roundabouts are an ideal location for a distinct turning manoeuvre and therefore a good place to identify the roll angle of the bicycle in the data.

Figure 17 shows the left turn into the roundabouts as a positive, 10-degree roll angle of for a short time followed by two, more distinct, negative roll angles of up to ~25 degrees. These last two represent the prolonged right hand turns in the hairpin bend on the second roundabout and on taking the third exit back at the first one. Interestingly, there is even evidence of possible counter steer in the lead up to each turn. Periods where the roll angle is small, or roughly zero, can be seen between each turn and are the sections of flat, level road connecting the two roundabouts. The author attributes the oscillatory nature of the estimations, often seen when on the flat roads, to the pronounced rolling motions caused by the pedalling style of the rider during testing.

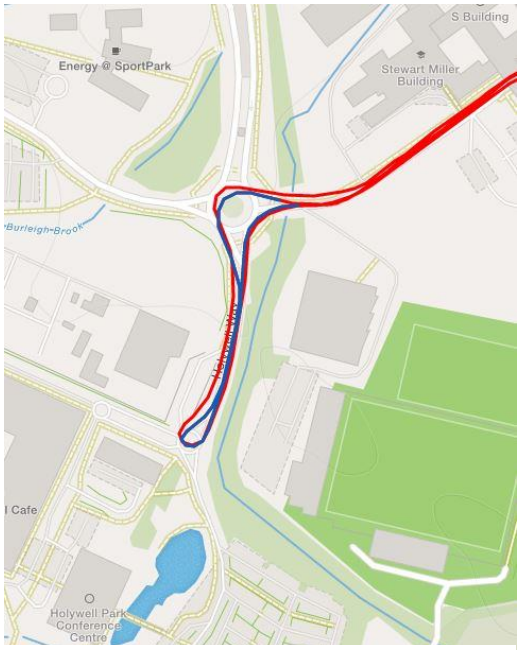

Figure 16 – West Park roundabouts navigated during testing.

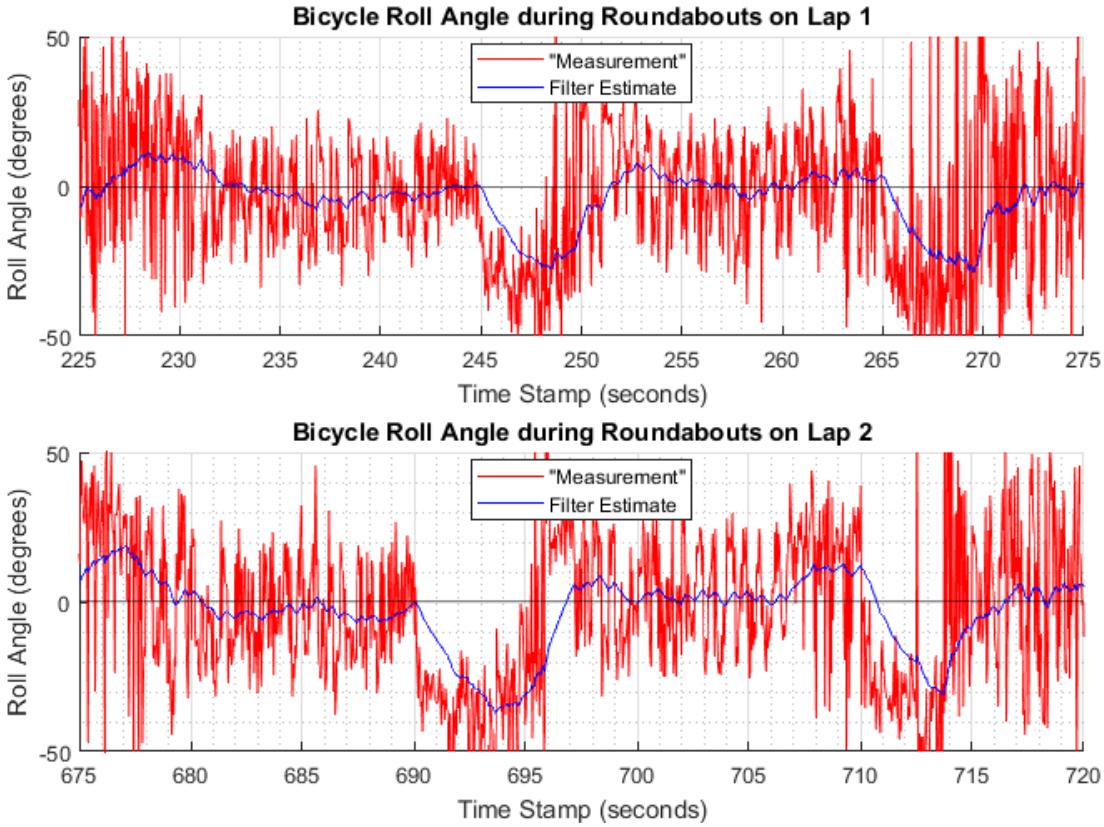

Figure 17 – The final roll angle estimation (blue) of a bicycle, navigating a pair of roundabouts in close succession, calculated by the filter using measurements of the virtual roll angle (red) and the gyroscope roll rate. Plots after each step of this process are available in the Appendix.

5.4.3 Performance Assessment using a Simulated Signal

To assess the performance of the Kalman Filter quantitatively, it is customary to use a simulated signal contaminated by noise and compare the result with a known truth. This assessment has been completed using data generated by the computational motorcycle model, as seen in section 3. The data is used to compute an estimation for the roll angle of the motorcycle using the same methods used throughout this section, and comparing it to a reference signal, the model's calculation of the roll angle in this case.

The "measurements" used from the model are the angular rates in the body co-ordinate system of the virtual motorcycle that are the simulation equivalent of the angular rates measured by the gyroscopes used in the practical field tests. The simulated measurements from each axial component were deliberately contaminated to reflect the noise components in the sensor measurements. There are two constituents to the contamination process applied to the measurements: noise generation and bias adjustment. Noise generation adds a random number to each measurement where the random number is normally distributed about a zero mean, with a standard deviation identical to that of the real sensor in each axis. As covered previously, the bias of the sensor is assumed to be constant and so the measurements are made biased by adding the bias value of the sensor in each axis.

After applying the same treatment for the actual measurements to the simulated signal, the measurements are filtered and results for the roll angle estimation are obtained, as shown in figure 18, whilst the results from each of the stages are included in the appendix. With a reference signal available this time, an analysis of the error can be performed, and this estimation method was calculated as having a root mean square error of 2.17 degrees which is close to the error claimed by the authors of the literature this technique is based on. The author advises that this validation be approached with some caveats in mind: the simulation is for a motorcycle, with properly modelled tyre dynamics and parameter vastly different to a bicycle, and that the roll angle remains both 'small' and constant for the entire simulation. A better simulation might simulate more variable roll angles in sustained turning manoeuvres.

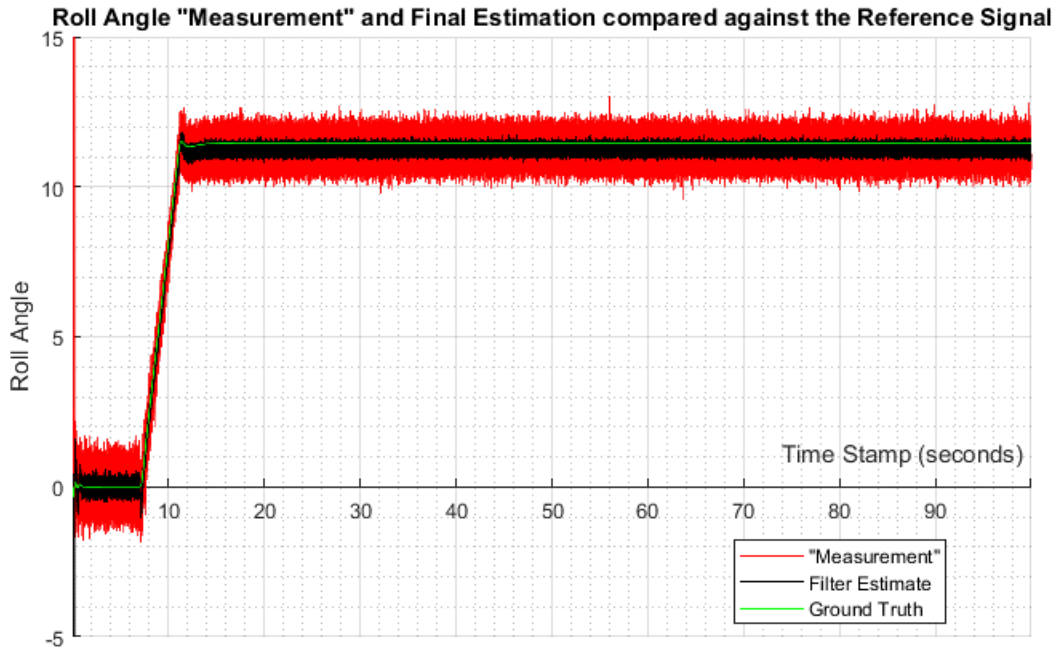

Figure 18 – Validation of the roll angle estimation method using simulated signals.

5.5 Results & Discussion

The results of the final roll angle estimation from the test data are very pleasing, showing consistent performance in straight and level travel as well as sustained turns, especially in such a dynamic test environment. However, there remain opportunities for further exploration that may offer even better performance. Additional time would be well spent experimenting with the tuning of the filter constants such as the covariance matrix of the plant noise, Q, and the constant, $\bar{\varphi}^2$, used to calculate the blending function co-efficient. Both of these were left to their default, or recommended, values from the literature and work well but could be revisited with more time available to study the effects of doing so.

Further validation of the method through additional experimentation might also be worth exploring possibly using a static test rig or rollers, a training device typically used by amateur racers to train, where both wheels are able to turn and the user is able to remain in place whilst freely balancing and pedalling at the same time. Comparing a known value for the roll angle against results from either of these methods would validate the method practically as well as computationally.

One drawback to this method, however, is its complexity and subsequent demand on resources computationally. The many stages of this process generate lots of variables that need to be stored on the working memory (RAM), a factor noted by the author as being limited throughout testing. Additional processing power is also recommended to perform the calculations satisfactorily without compromising the estimation rate required. In this project, 25 Hertz appears to work well although the author would ideally opt for up to 40 or 50 Hertz to give the control system a better perception of the attitude of the vehicle. Given the fundamental nature of the roll angle estimation as an input to the control system of this application, every opportunity to improve its accuracy, precision and reliability should be exploited.

6 Overall Summary and Conclusions

The work conducted by the author has made inroads into the two key areas required for an autonomous two wheeled vehicle - control of steering actuation and roll angle estimation. A computational model of a motorcycle has been adapted to include a DC motor for the application of steering torque as a function of the voltage supplied, allowing it to be controlled computationally and can be extended to automated control of the vehicle using PID control and state estimation.

Furthermore, a working, first-generation prototype for the electronic device required to measure the speed and roll angle of the vehicle has been produced and the author has identified the appropriate shortcomings of the sensor module required make improvements. Accompanying the sensor module are the relevant calculations and data processing algorithms that provide an estimation for the roll angle of the vehicle deemed satisfactory at this stage, though the effectiveness of these cannot be more conclusively validated until they are either tested in parallel with the control system and steering actuation or verified experimentally, as in the literature that inspires them.

From this point, remaining work in this area includes converting the model into a practical control system through a complete reparameterization process, adapting it from a motorcycle model to that of a bicycle. A DC motor and supporting electronics, are all that remain to be added to the device to provide the steering actuation. This addition can be considered modular to what has already been built since the appropriate infrastructure exists with this in mind which should make the process more straightforward.

Unification of said control system with the sensor module and a motor for steering actuation, followed by any subsequent retuning or refinement required after either of these two processes, is a simplification of the final necessary steps towards having a working vehicle ready to test and improve iteratively. The roll angle estimation calculations have been applied to the data and demonstrated offline in post process, however, ideally they would have to be computed in real time alongside the control system whilst the vehicle is in motion, something which may require additional computing resources than were used for this research.

The author acknowledges that his work can be refined further, like any engineering challenge, through continuous improvement of the existing research, building on the work of colleagues or through new, alternative approaches entirely. The door remains open for another individual, or team, to pick up where this project has ended and continue the work in these areas to achieve a functioning control system with actuation and commence working on the final requirement that is path navigation, which remains unexplored in the timeline of this project. Looking forward, the scope could even be widened to include computer vision and machine learning to further enhance the capabilities of the vehicle as well as any role this project could play in the field of autonomous vehicles. The author encourages any person that takes on this project to consider the shortcomings and suggested improvements detailed in this document, and, equally importantly, to enjoy the exploration process of each new opportunity presented by this project as much as he has.

Appendix – COVID-19 & Document Notes

COVID-19 Disruption

Fortunately, this project has not been disrupted *too* severely by the global coronavirus outbreak, the subsequent closure of university facilities and government advice to self-isolate within the home. A great deal of the work was able to continue at the author's home, however, the two main project objectives were reassessed and adjusted with the scope of the project narrowed accordingly in line with what could be realistically achieved under the circumstances. This section of the appendix details exactly how the project has been affected.

When talk of the closure of the university facilities first circulated, there was discussion between the author and the supervisor as to the possible implications of such a case, but no action was taken as it was not seen as necessary at the time. As soon as the closure was announced and stricter government advice was issued, the main objectives of the project, as outlined in the preparatory report, were re-evaluated and recategorised by the supervisor. After a discussion with the author they were reissued in order of priority as follows:

1. Kalman Filter
    - Apply the Kalman filter algorithm to the sensor module measurements to obtain a suitable estimate for the roll angle or attitude of the bicycle
2. Sensor Module
    - Design & test the roll angle and velocity sensor module
    - Carry out a field test to gather data using the sensor module
3. DC Motor & Motorcycle Model Integration
    - Complete modelling of a DC motor, with torque, as a function of supply voltage, as the desired control output,
    - Integrate said model into pre-existing motorcycle model
4. Complete tuning of PID gains, simulating the above model, for optimum performance
5. Adapt a pre-existing vehicle model to replicate true properties of the test bicycle

- ~~Design of balance control system~~
- ~~Design of steady-state turn control system~~
- ~~Re-assess the steering torque delivery mechanism and complete any reworking~~
- ~~Assemble the control system, sensor module & other components~~
- ~~Install the control system components on board the test vehicle~~

The author understands the circumstances prevented access to facilities required to complete certain objectives, that any expectation of such facilities to be made available to them personally or externally would be unreasonable and, as such, these objectives have been withdrawn accordingly. The remainder were to be completed as far as possible. Shortly after the university closure, meetings and regular communication with the supervisor have continued via internet alternatives and have not been negatively impacted. Although the author preferred the regular communication and accessibility, afforded by a physical campus presence, it was essential to accept that communication was going to be different under the circumstances.

Due to the computational nature of much of the project and the author having the suitable personal facilities available at home to complete this work, they were not significantly disadvantaged in this regard. The same can be said for the practical aspects of the project; the author was able to accomplish the design, construction and testing of the instrumentation module using the personal resources available to him or improvise if necessary. Ideally, access to some of the campus/department, fabrication facilities would have been preferable for reasons discussed in the primary sections of this document, but the author is confident that, where applicable, a suitable solution has been applied though improvisation or post process correction.

Document Notes

Introduction

Derivation from the Steady Turn Case & Small Roll Angle Approximation

The derivation for the roll angle calculation given in equation 4.

$$l = \overrightarrow{O\ CoM}$$

Centrifugal acceleration, a_y, is given by:

$$a_y = \frac{V^2}{R_c} \qquad (1.1)$$

Forward velocity can be written generally in terms of the radius of the turn and the rate of turn:

$$V = R\dot{\psi}$$

Meaning we can rewrite the centrifugal acceleration equation as:

$$a_y = \frac{V \times R_c\dot{\psi}}{R_c}$$

$$a_y = V\dot{\psi} \qquad (1.2)$$

For a steady state, the forces are balanced, and described as follows:

$$W = mg$$

$$F_{Rz} = -mg$$

$$F_C = ma_y$$

$$F_{Ry} = -ma_y$$

For a steady state, the sum of the moments about the centre of mass are equal to zero;

Resolving perpendicular to *z'* / parallel to *y'*:

$$\Sigma \mathrm{M}_{y'} = 0$$

$$-\left(mg\sin\varphi + ma_y\cos\varphi\right) \times 0 + \left(F_z\sin\varphi + F_y\cos\varphi\right) \times l = 0$$

$$F_z\sin\varphi + F_y\cos\varphi = 0$$

$$-mg\sin\varphi - ma_y\cos\varphi = 0$$

$$-g\sin\varphi = a_y\cos\varphi$$

Ignoring the sign and employing trigonometric identities, we can write:

$$\tan\varphi = \frac{a_y}{g}$$

$$\varphi = \tan^{-1}\left(\frac{a_y}{g}\right) \qquad (2)$$

Using equations 1.1 & 1.2, equation 4 can expressed 5 & 6:

$$\varphi = \tan^{-1}\left(\frac{V\dot{\psi}}{g}\right) \qquad (3)$$

$$\varphi = \tan^{-1}\left(\frac{V^2}{R_c g}\right) \qquad (4)$$

Bicycle Instrumentation Module

Bias Test – Raw & Corrected Data

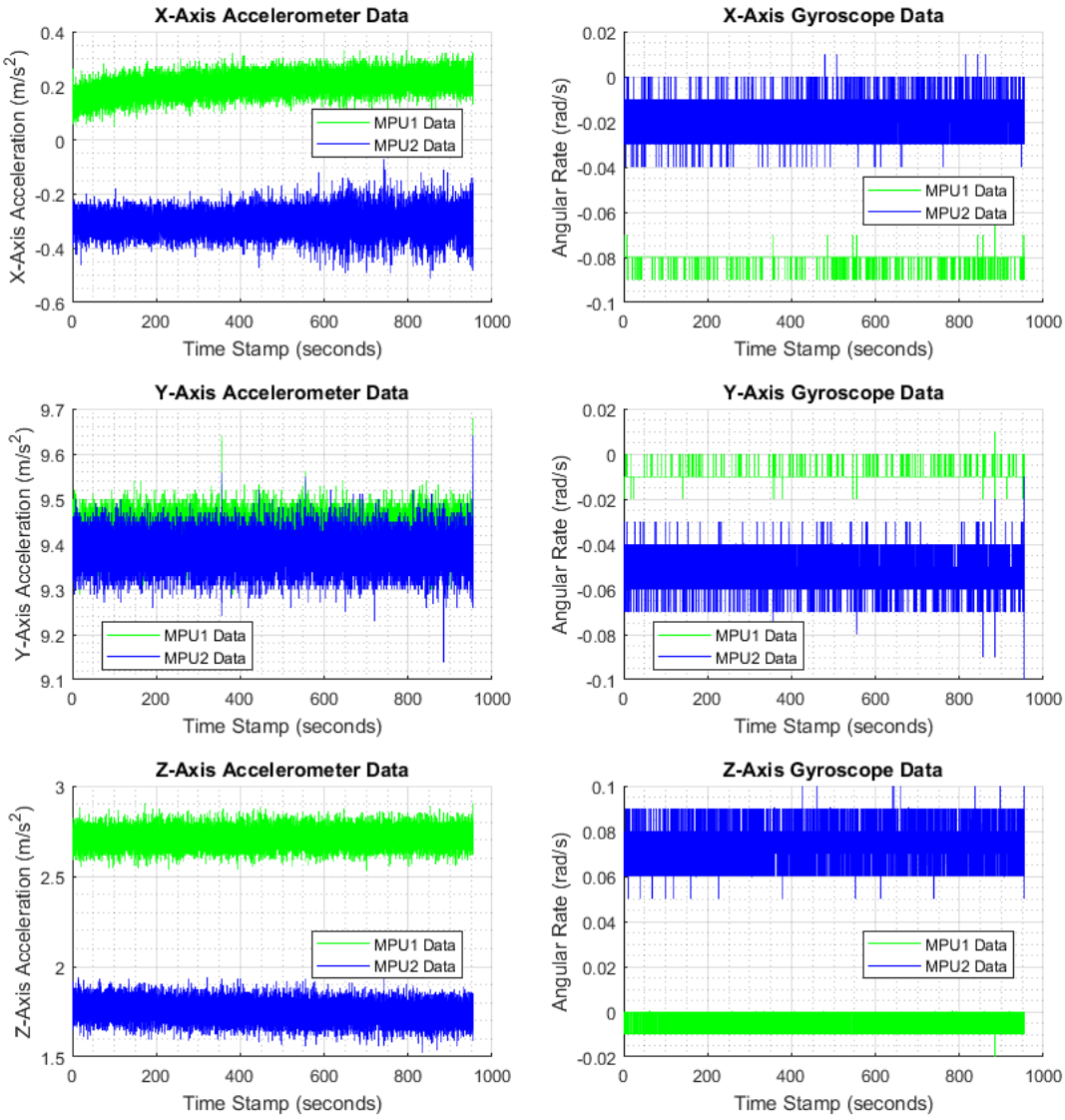

Figure 19 – Raw, unprocessed measurements from the static bias test of the instrumentation device. The process for gathering this data is detailed in section 4.4.2.

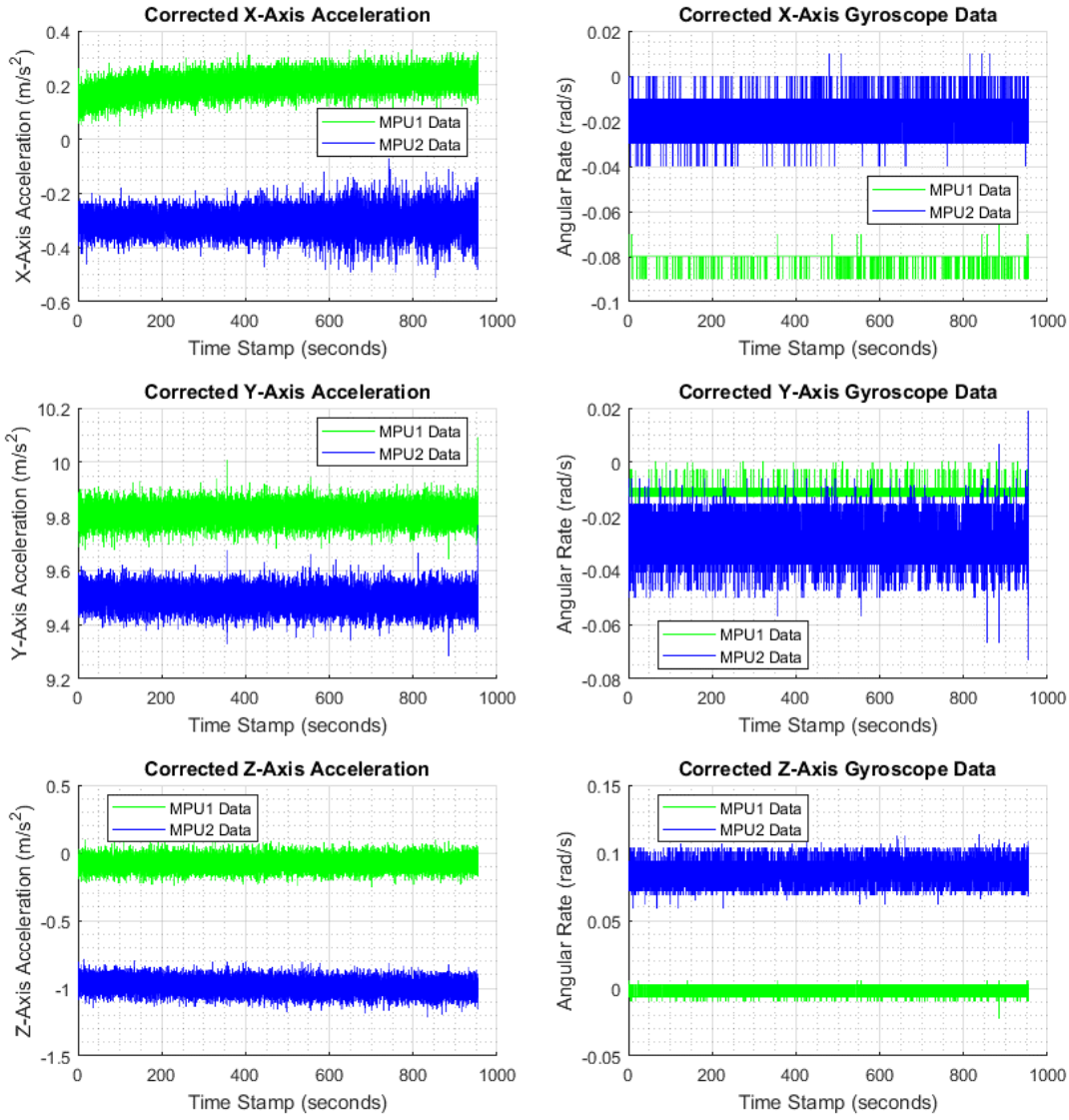

Figure 20 – Corrected measurements from the static bias test of the instrumentation device, the correction process for which is outlined in section 4.4.3 and equation 17.

Orientation Test – Raw & Corrected Data

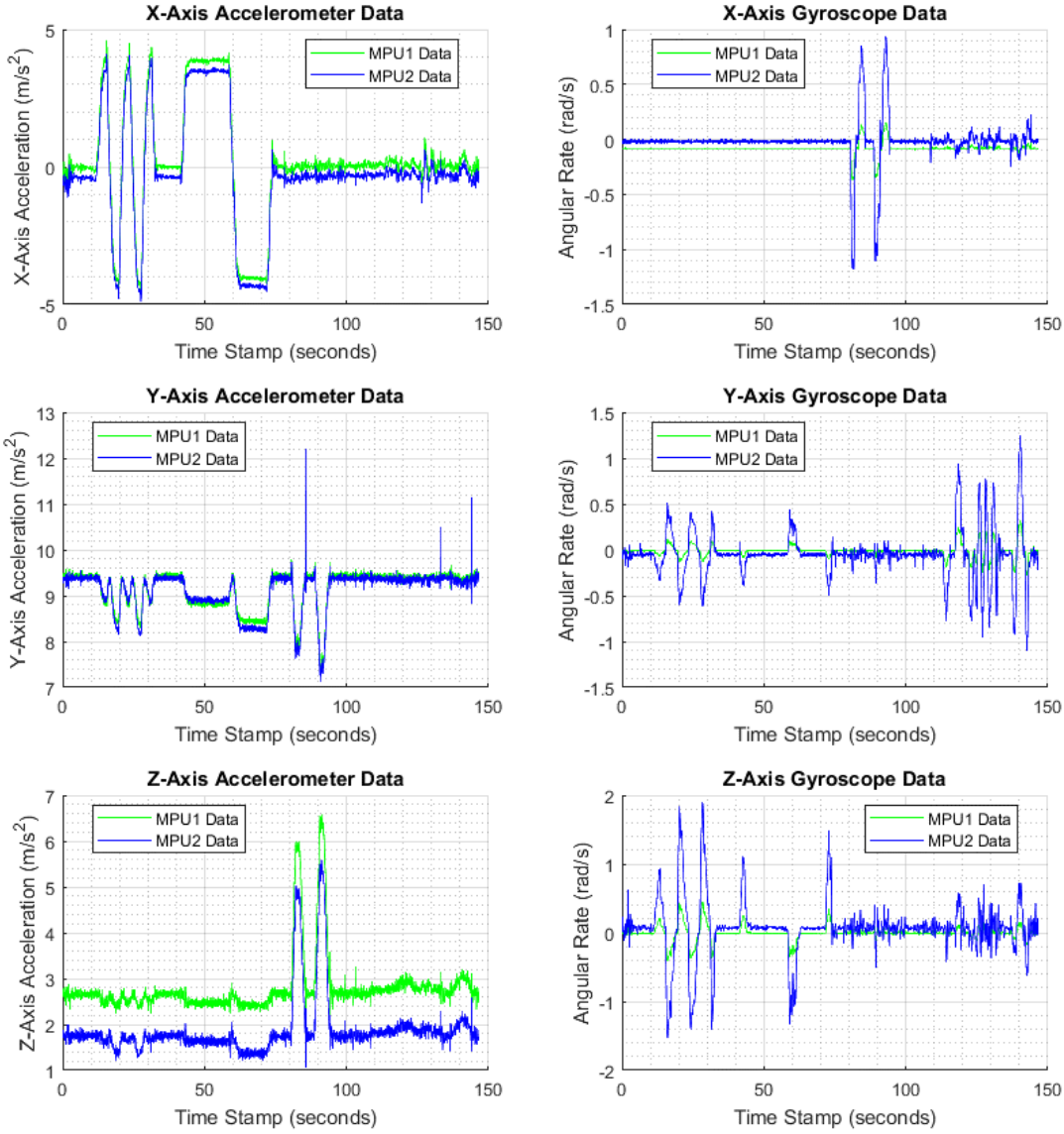

Figure 21 – Raw, unprocessed measurements from the static orientation test of the instrumentation device. The process for gathering this data is detailed in section 4.4.3.

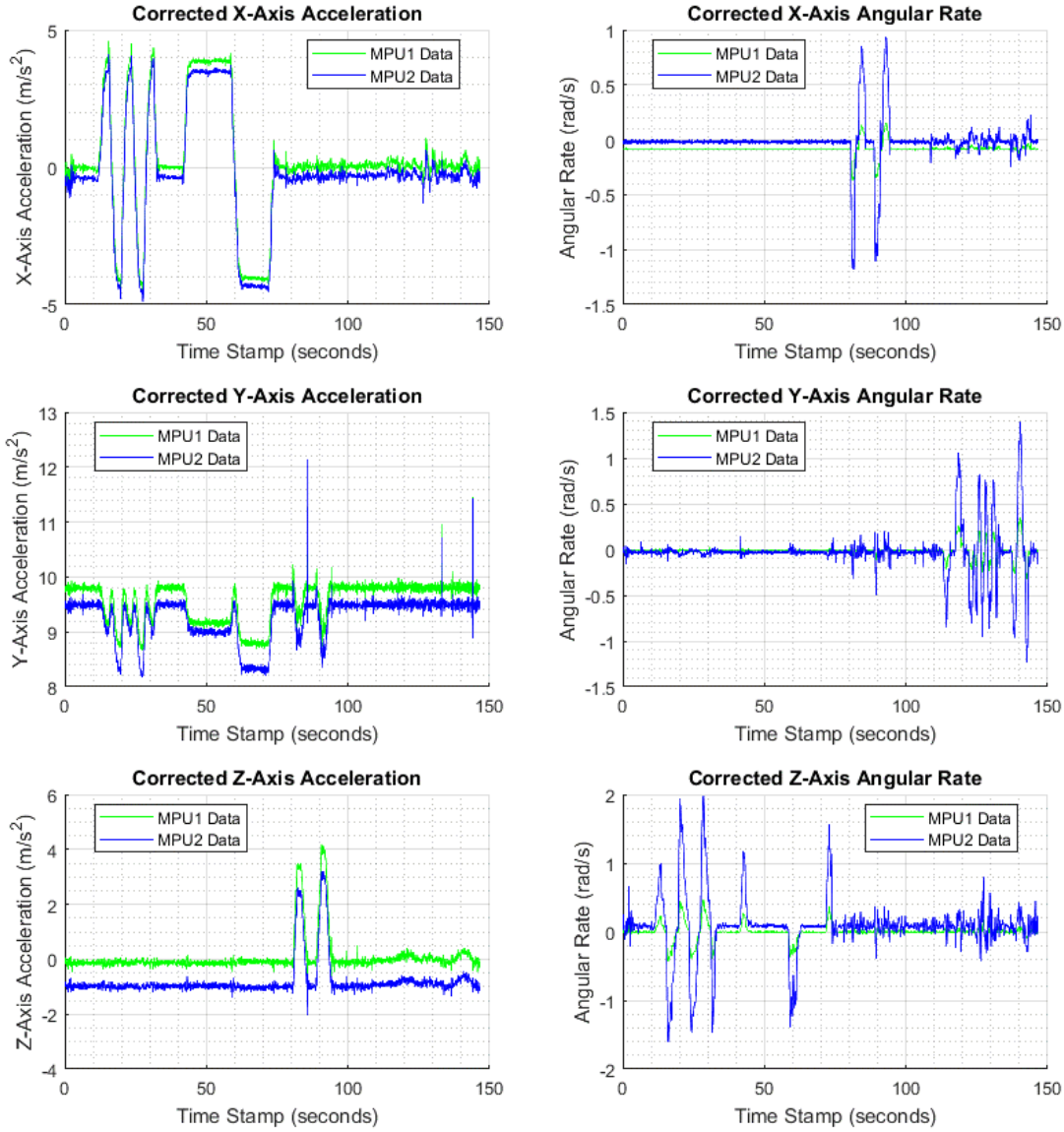

Figure 22 – Corrected measurements from the static orientation test of the instrumentation device, the correction process for which is outlined in section 4.4.3 and equation 17.

Kalman Filter – Results from each step of the Roll Angle Estimation Process Using Field Test Data

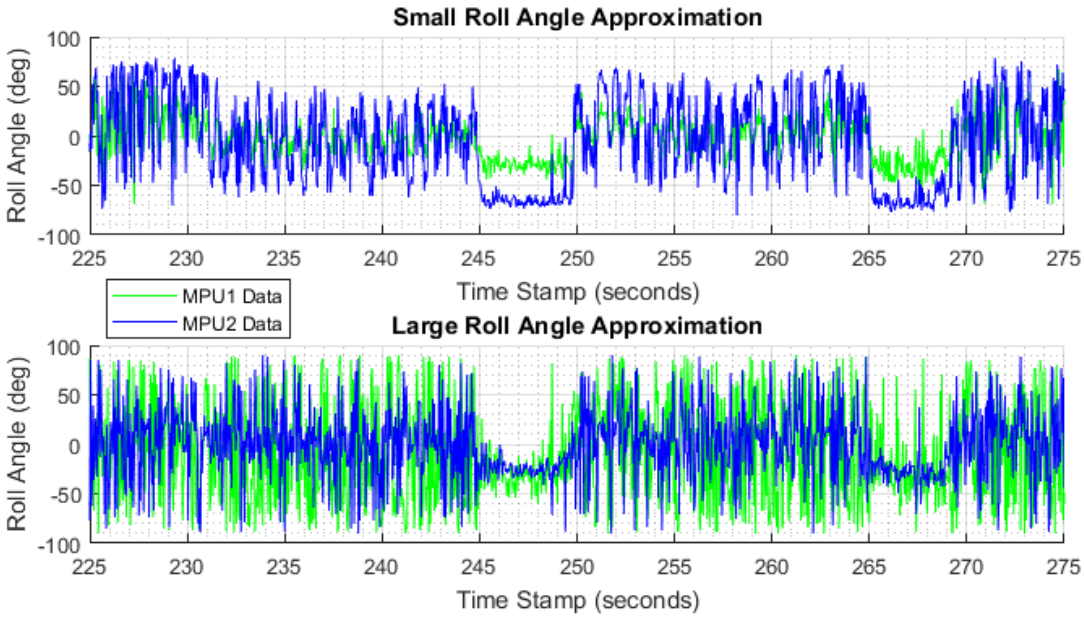

Figure 23 – Small and Large Roll Angle Approximations using corrected data from each sensor during the first passage of the roundabouts, navigated in the field test of the instrumentation device.

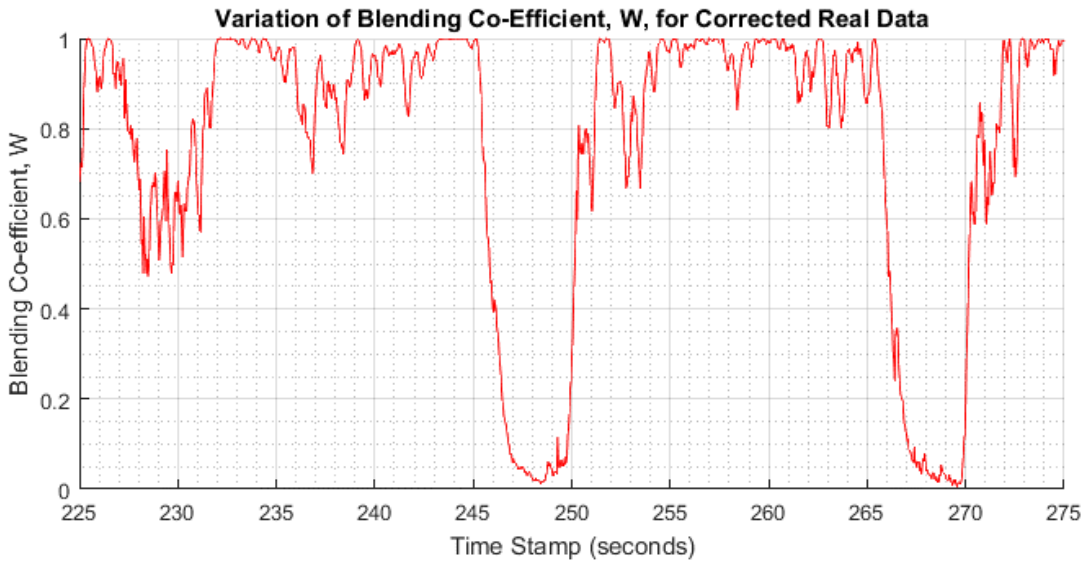

Figure 24 – The variation in the blending function co-efficient, W, during the application of the blending function in the Kalman filter and roll angle estimation process. The time period is the same as in the previous figure.

Using a Simulated Signal

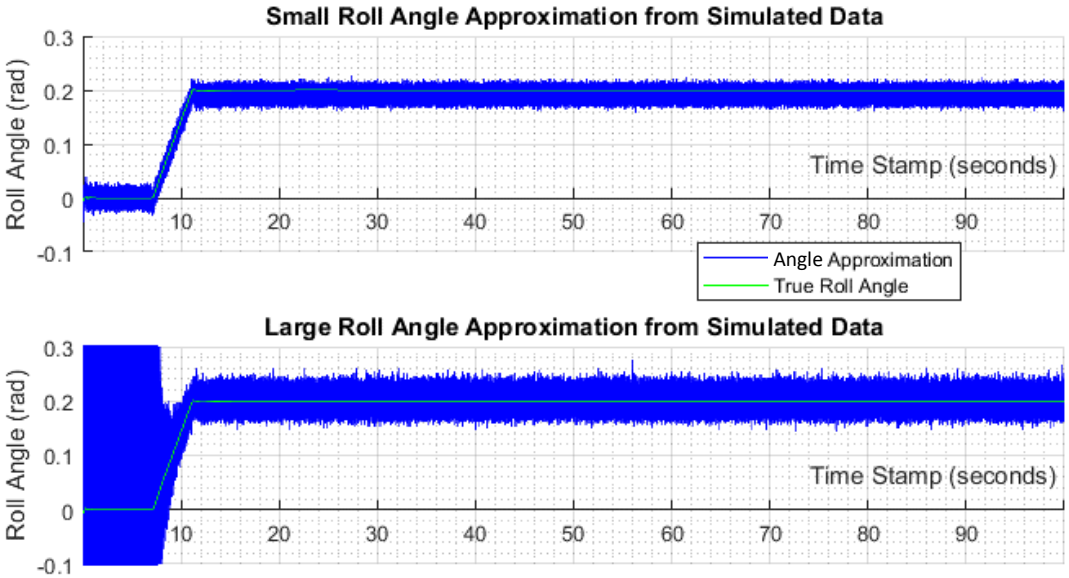

Figure 26 – Small and Large Roll Angle Approximations calculated from a simulated signal.

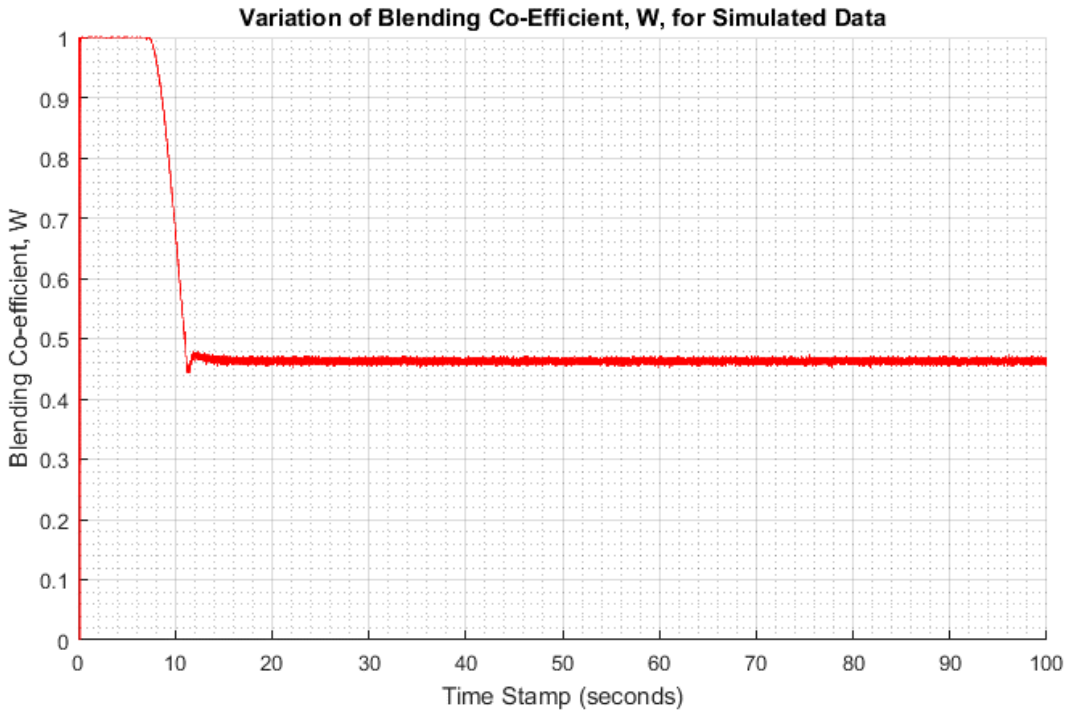

Figure 25 - The variation in the blending function co-efficient, W, during the application of the blending function in the Kalman filter and roll angle estimation process for the signal.

Code & Data

Sensor module code, static test & field test measurements and the data processing script may be downloaded and referred to using this link: github.com/rendersv/TTC003.git

Acknowledgments

The author extends special recognition and gratitude to the project supervisor, George Mavros, for providing an enjoyable learning experience in some challenging and unique circumstances in 2020. In addition to providing support in academic capacities, George also supported the author during a time which included some difficult personal circumstances. He has been encouraging throughout and played a large role in helping the author to not only further develop academically but also enjoy the last academic year of his degree.

References

1. S.S. Wilson, Mar. 1973. "*Bicycle Technology*". In: *Scientific American*, 228(3), 81-91.
2. D.G. Wilson, J.M. Papadopoulos, 2004. "*Bicycling Science*", 3rd Ed., The Massachusetts Institute of Technology Press.
3. TfL (2011-2012) London Travel Demand Survey: TfL in "*Roads Task Force – Technical Note 14*", http://content.tfl.gov.uk/technical-note-14-who-travels-by-car-in-london.pdf.
4. B. Plowden, A. Bristow, Nov. 2016. "*Update on the implementation of the Quietways and Cycle Superhighways programmes*", TfL Programmes and Investment Committee, http://content.tfl.gov.uk/pic-161130-07-cycle-quietways.pdf.
5. TfL Report, 2018. "*Travel in London*", 11th Ed., p. 142., http://content.tfl.gov.uk/travel-in-london-report-11.pdf.
6. V. Cossalter, R. Lot, M. Massaro, 2006. *"Motorcycle Dynamics",* 2nd Ed., in: M. Tanelli, M. Corno, S.M. Savaresi, 2014. "*Modelling Simulation and Control of Two-Wheeled Vehicles*", 1st Ed. John Wiley & Sons Ltd., p. 3 – 42.
7. K. Zhang, T.J. Sejnowski, 1999. "*A theory of geometric constraints on neural activity for natural three- dimensional movement*", The Journal of Neuroscience: the official journal of the Society for Neuroscience. 19. 3122-45.
8. F.J.W. Whipple, 1899. "*The stability of the motion of a bicycle*" in: *Quarterly Journal of Applied Mathematics Vol. 30*, p. 312 – 348.
9. S. Timoshenko, D.H. Young, 1948. "*Advanced Dynamics*" p. 243.
10. J.P. Meijaard, J.M. Papadopoulos, A. Ruina, A.L. Schwab, 2007. "*Linearized dynamics equations for the balance and steer of a bicycle: A benchmark and review*" in: *Proc. R. Soc. A* (2007) 463, p. 1955 – 1982.
11. D.E.H. Jones, 1970. "*The stability of the bicycle*" in: *Physics Today* (April) p. 34 – 40.
12. J. P. Meijaard, J.M. Papadopoulos, A. Ruina, A. L. Schwab, 2011. "*Historical Review of Thoughts on Bicycle Self-Stability*", published on Cornell E-commons: http://ecommons.library.cornell.edu/handle/1813/22497
13. J.D.G. Kooijman, J. P. Meijaard, J.M. Papadopoulos, A. Ruina, A. L. Schwab, 2011. "*A Bicycle Can Be Self-Stable Without Gyroscopic or Caster Effects*" in: *Science* 15 Apr 2011: Vol. 332, Issue 6027, p. 339 – 342.

14. J.D.G. Kooijman, J. P. Meijaard, A. L. Schwab, 2007. "*Experimental validation of a model of an uncontrolled bicycle*" in: *Multibody System Dynamics* 2008: Vol. 19, p. 115 – 132.
15. W.J.M. Rankine, 1869. "*On the dynamical principles of the motion of velocipedes*" in: *The Engineer* (1870).
16. J.M. Papadopoulos, 1987. "*Bicycle steering dynamics and self-stability: A summary report of work in progress.*" Cornell Bicycle Project Report, Dec. 15.
17. G. Mavros, 2019. "*LAB SESSION: Motorcycle and rider model.*" In: *TTD017 Vehicle Handling* Module Resources, Department of Aeronautical and Automotive Engineering, Loughborough University, Loughborough.
18. M. Best, 2019. "*TTD017 Vehicle Handling Course Notes.*" In: *TTD017 Vehicle Handling* Module Resources, Department of Aeronautical and Automotive Engineering, Loughborough University, Loughborough.
19. S. Miah, E. Milonidis, I. Kaparias, N, Karcanias, 2019. "*An Innovative Multi-Sensor Fusion Algorithm to Enhance Positioning Accuracy of an Instrumented Bicycle*." In: *IEEE Transactions on Intelligent Transportation Systems*, p. 1 – 9.
20. E. Sanjurjo, M.A. Naya, J. Cuadrado & A.L. Schwab, 2019. "*Roll angle estimator based on angular rate measurements for bicycles.*" In: *Vehicle System Dynamics* 57:11, 1705 – 1719.
21. S.M. Cain & N.C. Perkins, 2012. "*Comparison of experimental data to a model for bicycle steady-state turning,*" *Vehicle System Dynamics*, 50:8, 1341 – 1364.
22. R. Lot, V. Cossalter, M. Massaro, 2012. "*Real-time roll angle estimation for two-wheeled vehicles*" in *Proceedings of the ASME 2012 11th Biennial Conference on Engineering Systems Design and Analysis*.
23. G. Mavros, 2017. "*Electrotechnology Notes*", TTB211 Module Notes, Department of Aeronautical and Automotive Engineering, Loughborough University, Loughborough.
24. G.F. Franklin, 2010. "*Feedback Control of Dynamic Systems*", 6th Ed., Pearson Prentice Hall (Pearson Education, Inc.).
25. V.J. Renders, Jan. 2020. "*TTC003 – Final Year Project Preparation Report*". Supervised by G. Mavros. Undergraduate coursework submission to Department of Aeronautical and Automotive Engineering, Loughborough University, Loughborough.
26. *Canyon Bicycles GmbH* – Source for the Geometry & Dimensions data of the test bicycle: https://www.canyon.com/en-gb/road-bikes/race-bikes/ultimate/ultimate-cf-sl-frameset-mechanical/1186.html?dwvar_1186_pv_rahmenfarbe=BK%2FWH&quantity=1#!accordions=0_1

Bibliography

1. H.B. Pacejka, 2006. *"Tyre and Vehicle Dynamics"*, 2nd Ed., Butterworth-Heinemann/Elsevier.
2. H.B. Mitchell, 2012. *"Data Fusion: Concepts & Ideas"*, 2nd Ed., Springer-Verlag Berlin Heidelberg.